

Functional Data Representation with Merge Trees

Matteo Pegoraro* Piercesare Secchi†

August 28, 2022

Abstract

In this paper we face the problem of representation of functional data with the tools of algebraic topology. We represent functions by means of merge trees and this representation is compared with that offered by persistence diagrams. We show that these two tree structures, although not equivalent, are both invariant under homeomorphic reparametrizations of the functions they represent, thus allowing for a statistical analysis which is indifferent to functional misalignment. We employ a novel metric for merge trees and we prove a few theoretical results related to its specific implementation when merge trees represent functions. To showcase the good properties of our topological approach to functional data analysis, we first go through a few examples using data generated *in silico* and employed to illustrate and compare the different representations provided by merge trees and persistence diagrams, and then we test it on the Aneurisk65 dataset replicating, from our different perspective, the supervised classification analysis which contributed to make this dataset a benchmark for methods dealing with misaligned functional data.

Keywords: functional data analysis, functional alignment, merge trees, tree edit distance, topological data analysis.

1. Introduction

Since the publication of the seminal books by Ramsay and Silverman (Ramsay and Silverman, 2005) and Ferraty and Vieu (Ferraty and Vieu, 2006), Functional Data Analysis (FDA) has become a staple of researchers dealing with data where each statistical unit is represented by the measurements of a real random variable observed on a fine grid of points belonging to a continuous, often one dimensional, domain D . In FDA these individual data are better represented as the sampled values of a function defined on D and with values in \mathbb{R} . Hence, at the onset of any particular functional data analysis stands the three-faceted problem of *representation*, described by: (1) the smoothing of the raw and discrete individual data to obtain a functional descriptor of each unit in the data set, (2) the identification of a suitable embedding space for the sample of functional data thus obtained and, finally, (3) the eventual alignment of these functional data consistently with the structure of the embedding space. As a reference benchmark of the typical FDA pipeline applied to a real world dataset, we take the paper by Sangalli et al. (2009b) where the first functional data analysis of the AneuRisk65 dataset is illustrated.

Smoothing is the first step of a functional data analysis. For each statistical unit, individual raw data come in the form of a discrete set of observations regarded as partial observations of a function. Smoothing is the process by means of which the analyst generates the individual functional object out of the raw data. This functional object will be the atom of the subsequent analysis, a point of a functional space whose structure is apt to

*. MOX – Department of Mathematics, Politecnico di Milano

†. MOX – Department of Mathematics, Politecnico di Milano

sustain the statistical analysis required by the problem at hand. A common approach to obtain functional representations is to fit the data with a member of a finite dimensional functional space generated by some basis, for instance, splines or trigonometric polynomials. Signal-to-noise ratio and the degree of differentiability required for the functional representation, as well as the structure of the embedding space, drive the smoothing process. Functional representations interpolating the raw data are of no practical use when the analysis requires to consider functions and their derivatives or, for instance, the natural embedding space is Sobolev's; see, for instance, Sangalli et al. (2009a) for a detailed analysis of the trade-off between goodness of fit and smoothness of the functional representation when dealing with the Aneurisk65 dataset.

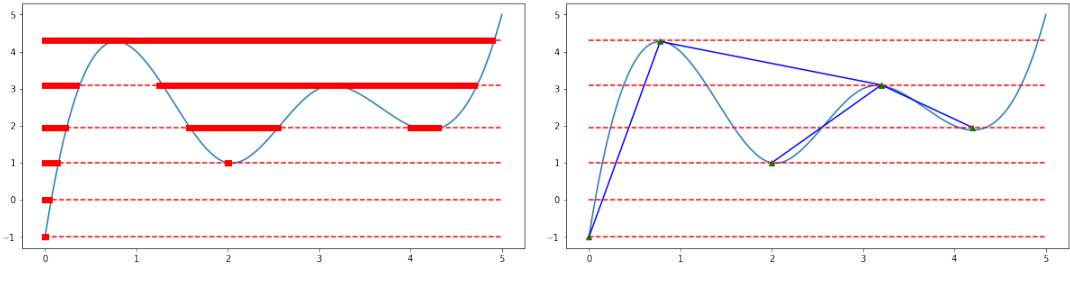
Functional data express different types of variability (Vantini, 2009) which the analyst might want to decouple before carrying on the statistical analysis. Indeed the Aneurisk65 dataset is by now considered a benchmark for methods aimed at the identification of *phase* and *amplitude variation* (see the Special Section on Time Warpings and Phase Variation on the Electronic Journal of Statistics, Vol 8 (2), and references therein). In many applications phase variation captures ancillary non-informative variability which could alter the results of the analysis if not properly taken into account (Lavine and Workman, 2008; Marron et al., 2014). A common approach to this issue is to embed the functional data in an appropriate Hilbert space where equivalence classes are defined, based on a notion of *alignment* or *registration*, and then to look for the most suitable representative for any of these classes (Marron et al., 2015). Such approach evokes ideas from shape analysis (Dryden and Mardia, 1998) and pattern theory (Ripley and Grenander, 1995), where configurations of landmark points are identified up to rigid transformations and global re-scalings. In close analogy with what has been done for curves (Michor et al., 2007; Srivastava et al., 2010), functions defined on compact real intervals D are aligned by means of warping functions mapping D into another interval, that is, they are identified up to some re-parametrization. Different kinds of warping functions have been investigated: affine warpings are studied for instance in Sangalli et al. (2010) while more general diffeomorphic warpings have been introduced in Srivastava et al. (2011). Once the *best* representatives are selected, the analysis is carried out on them leveraging the well behaved Hilbert structure of the embedding space. Classically, the optimal representatives are found by minimizing some loss criterion with carefully studied properties (Sangalli et al., 2014). This approach however has some limitations, arising from the fact that the metric structure of the embedding space might not be compatible with the equivalence classes collecting aligned functions (Yu et al., 2013). An alternative is to employ metrics directly defined on equivalence classes of functions such as the Fisher Rao metric, originally introduced for probability densities (Srivastava et al., 2007), which allows for the introduction of diffeomorphic warpings (Srivastava et al., 2011). It must be pointed out that all these ways of dealing with the issue of ancillary phase variability encounter some serious challenges when the domain D is not a compact real interval.

A different approach to the problem of phase variation is to capture the information content provided by a functional datum by means of a statistic which is insensitive to the functional data re-parametrization, but sufficient for the analysis. Algebraic topology can help since it provides tools for identifying information which is invariant to deformations of a given topological space (Hatcher, 2000). Topological Data Analysis (TDA) is a quite recent field in data analysis and consists of different methods and algorithms whose foundations rely on the theory developed by algebraic topology (Edelsbrunner and Harer, 2008). The main source of information collected by TDA algorithms are homology groups (see, for instance, Hatcher (2000)) with fields coefficients which, roughly speaking,

count the number of holes (of different kinds) in a topological space. For instance zero dimensional holes are given by path connected components and one dimensional holes are given by classes of loops (up to continuous deformations) which cannot be shrunk to one point. One of the most interesting and effective ideas in TDA is that of *persistent homology* (Edelsbrunner et al., 2002): instead of fixing a topological space and extracting the homology groups from that space, a sequence of topological spaces is obtained along various pipelines, and the evolution of the homology groups is tracked along this sequence. The available pipelines are many, but the one which is most interesting for the purposes of this work is that concerning real valued functions. Let the domain D be a topological space X and consider a real valued function defined on X , $f : X \rightarrow \mathbb{R}$. One can associate to f the sequence of topological spaces given by the sublevel sets $X_t = f^{-1}((-\infty, t])$, with t ranging in \mathbb{R} . The evolution of the connected components along $\{X_t\}_{t \in \mathbb{R}}$ is thus analysed for the purpose of generating a topological representation of f .

In this work, we consider specific topological representations of f constructed along this general scheme and we show that they are invariant with respect to homeomorphic warpings of the domain X . Moreover, these representations are also able to separate big shape features of f from small oscillations; the overall shape of the function captured by the topological representations we will deal with is unaffected by the presence of smaller oscillations, which are captured as well, but separately. These two properties make the TDA approach pursued in this manuscript a candidate for the representation of functional data, indeed a robust competitor able to deal in a natural way with phase variation and insensitive to the fine tuning of the preliminary smoothing phase, since functional features likely generated by overfitted representations are easily identified as ancillary in the subsequent topological representation.

To allow for the statistical analysis of functional data summarised by their topological representations, we need to embed the latter in a metric space. The choice of persistence diagrams (PD) (Cohen-Steiner et al., 2007) as summaries obtained through persistent homology drives many successful applications (Xia et al., 2016; Bhattacharya et al., 2015; Pokorný et al., 2015; Chung et al., 2009; Wang et al., 2018; Kramár et al., 2013), although other topological summaries are in fact known in the literature (Bubenik, 2015; Adams et al., 2017; Chazal et al., 2015). In this work we exploit a topological alternative – not equivalent – to a persistence diagram, called *merge tree*. Merge trees representations of functions are not new (Morozov and Weber, 2013) and are obtained as a particular case of Reeb Graphs (Shinagawa et al., 1991; Biasotti et al., 2008). Different frameworks have been proposed to work with merge trees (Beketayev et al., 2014; Morozov et al., 2013), mainly defining a suitable metric structure to compare them (Gasparovic et al., 2019; Touli, 2020). However all such metrics have a very high computational cost, causing a lack of examples and applications even when approximation algorithms are available (Touli and Wang, 2018), or they require complex workarounds to be effectively used (Sridharamurthy et al., 2020). We employ the metric for merge trees introduced in [\[Paper Metriche\]](#), showing that its computational complexity is reasonable when the trees involved are not too large. When working with representations of data, it is fundamental to study the behaviour of the operator which maps the single datum into the chosen representation to assess which kind of information is transferred from the initial data to the space of representations. For this reason we develop a new theoretical analysis on the stability/continuity of merge trees with respect to perturbations of the original functions. We also carry out examples to showcase differences between merge trees and persistence diagrams of functions. Having devoted the initial sections of the paper to the understanding of the behaviour of these



(a) Sublevel sets of a function (b) A function with its associated merge tree.

topological tools, we finally tackle, with our TDA approach, the benchmark functional classification case study detailed in Sangalli et al. (2009b).

The paper is organized as follows. In Section 2, we introduce the merge tree representation of a function. In Section 3 we briefly recall the definition of persistence diagrams in order to draw, in Section 4, some comparison between them and merge trees, before proving the invariance property which holds true for both topological representations. In Section 5 we present the metric structure for the space of merge trees which is used in the examples and in the final case study. In Section 6 we investigate the continuity properties of the operator which assigns to a function its merge tree, with respect to the aforementioned metric. After a short Section 7 on a visualization trick for the graphical representation of merge trees, in Section 8 we propose some *in silico* examples for illustrating differences and similarities between persistence diagrams and merge trees. Lastly, in Section 9, we tackle the functional data classification problem explored in Sangalli et al. (2009b) and we compare their results with those obtained following the TDA approach we advocate in this paper. We finally conclude the manuscript with a discussion, in Section 10, which points out some ideas pertaining our topological approach to functional data analysis. Appendix A collects the proofs of the results of the paper.

2. Merge Trees of Functions

We now define the merge tree representation of a function. Merge trees are an already established tool in topology and, to some extent, also in statistics since dendrograms can be regarded as merge trees. Nevertheless, we are going to spend a few lines to define them, so that the definition fits into the framework defined in [\[Paper Metriche\]](#), which differs from the classical one, found for instance in Morozov and Weber (2013). Roughly speaking, the pipeline to obtain a merge tree is the following: we transform the given function into a sequence of nested subsets and then we track the topological changes along this sequence. Such information is then turned into a tree.

The details are described in the following subsections.

2.1 Sublevel Sets

Consider a function $f : X \rightarrow \mathbb{R}$, with X being any topological space. We call sublevel set at height $t \in \mathbb{R}$, the set $X_t := f^{-1}((-\infty, t]) \subset X$. The key property of the family $\{X_t\}_{t \in \mathbb{R}}$ is that such subsets are nested: if $t \leq t'$ then $X_t \subset X_{t'}$. Note that the sequence $\{X_t\}_{t \in \mathbb{R}}$ is fully determined by the shape of the function f ; see Figure 1a. In fact, for $x \in X$, $f(x) = \inf_{t \in \mathbb{R}} \{t \text{ such that } x \in X_t\}$, hence no information carried by f is lost by its representation $\{X_t\}_{t \in \mathbb{R}}$.

2.2 Path Connected Components

A topological space X is path connected if for every couple of points $x, y \in X$ there is a continuous curve $\alpha : [0, 1] \rightarrow X$ such that $\alpha(0) = x$ and $\alpha(1) = y$. The biggest path connected subsets contained in a topological space are called path-connected components. Path connected components are the source of information we want to track along the sequence $\{X_t\}_{t \in \mathbb{R}}$.

Given $X_t \subset X$ we call $\mathbb{U}^t = \{U_i^t\}_{i \in I}$ the set of its path-connected components, which is indexed by some set I . We will make some very strict assumptions on such I but for now we do not need them. The main fact about path connected components is that if $X_t \subset X_{t'}$, then, for every i , there is a unique j such that $U_i^t \subset U_j^{t'}$.

Thus, we can define:

$$\alpha_t^{t'} : \mathbb{U}^t \rightarrow \mathbb{U}^{t'}$$

such that

$$U_i^t \subset \alpha_t^{t'}(U_i^{t'})$$

for all $U_i^t \in \mathbb{U}^t$.

A $t \in \mathbb{R}$ is called *critical value* if, for every $\varepsilon > 0$, $\alpha_{t-\varepsilon}^t$ is not bijective.

2.3 Tree Structures

Following [\[Paper Metriche\]](#), we now define what we mean with *tree* and with *merge tree*.

Definition 1 A tree structure T is given by a set of vertices V_T and a set of edges $E_T \subset V_T \times V_T$ which form a connected rooted acyclic graph. We indicate the root of the tree with r_T . We say that T is finite if V_T is finite. The order of a vertex of T is the number of edges which have that vertex as one of the extremes. Any vertex with an edge connecting it to the root is its child and the root is its father: this is the first step of a recursion which defines the father and children relationship for all vertices in V_T . The vertices with no children are called leaves or taxa. The relation father > child induces a partial order on V_T . The edges in E_T are identified in the form of ordered couples (a, b) with $a < b$. A subtree of a vertex v is the tree structure whose set of vertices is $\{x \in V_T | x \leq v\}$.

Definition 2 A finite tree structure T coupled with a monotone increasing height function $h_T : V_T \rightarrow \mathbb{R}$ is called *merge tree*.

Let us see how, starting from a real valued function $f : X \rightarrow \mathbb{R}$, we can represent it by means of a merge tree. We use the following notation: given a finite set C , then $\#C$ is its cardinality.

Consider $f : X \rightarrow \mathbb{R}$, and assume X to be a path connected topological space and f a *tame* function. We recall that a function is tame if for every X_t , the set \mathbb{U}^t is finite and along the sequence $\{X_t\}_{t \in \mathbb{R}}$ there are only a finite set of critical values. The idea is that, since path-connected components in every X_t can only arise, merge with others, or stay the same, it is quite natural to represent this merging structure with a tree structure. However, a tree structure T is not enough to represent the information contained in \mathbb{U}^t and $\alpha_t^{t'}$, so we also define a monotone increasing height function $h_T : V_T \rightarrow \mathbb{R}$ which encodes the critical values $t_0 < \dots < t_n$ of f .

The tree structure T and the height function h_T are built along the following rules:

- set a leaf with height t_0 for every element in \mathbb{U}^{t_0} ;
- for every $U \in \mathbb{U}^{t_{i+1}}$ such that $U \notin \text{Im}(\alpha_{t_i}^{t_{i+1}})$, set a leaf with height t_{i+1} ;

- for every t_i such that $\alpha_{t_i}^{t_{i+1}}(U) = \alpha_{t_i}^{t_{i+1}}(U')$, with U and U' in \mathbb{U}^{t_i} , set a vertex with height t_{i+1} , where vertices associated to $(\alpha_{t_i}^{t_i})^{-1}(U)$ and $(\alpha_{t_i}^{t_i})^{-1}(U')$ merge. With $t^U = \min\{t_j \mid \#(\alpha_{t_j}^{t_i})^{-1}(U) = 1\}$ and $t^{U'} = \min\{t_j \mid \#(\alpha_{t_j}^{t_i})^{-1}(U') = 1\}$.

The last merging happens at height t_n and, since X is path connected, at height t_n there is only one point, which is the root of the tree structure.

Look at Figure 1b for a first example. The height function is given by the dotted red lines. We can appreciate that the merge tree of f is heavily dependent on the shape of f , in particular on the displacement of its maxima and minima.

2.4 Isomorphism classes

Before continuing we must decide on the topological information which we regard as equivalent. In other words, which merge trees we want to distinguish and which we do not. This step is essential and decisive to tackle the phase variation problem presented in the introduction: to select information that is insensitive to some kind of transformation amounts to defining classes of functions which are represented by the same tree. We opt for a very general solution: we remove from the vertices of the tree any information regarding the connected components they are associated to, for instance, size, shape, position, the actual points contained etc..

Definition 3 *Two tree structures T and T' are isomorphic if there exists a bijection $\eta : V_T \rightarrow V_{T'}$ inducing a bijection between the edges sets E_T and $E_{T'} : (a, b) \mapsto (\eta(a), \eta(b))$. Such η is an isomorphism of tree structures.*

Definition 4 *Two merge trees (T, h_T) and $(T', h_{T'})$ are isomorphic if T and T' are isomorphic as tree structures and the isomorphism $\eta : V_T \rightarrow V_{T'}$ is such that $h_T = h_{T'} \circ \eta$. Such η is an isomorphism of merge trees.*

The rationale behind Definition 3, and the equivalence classes of isomorphic merge trees it generates, is analogous to that moving the introduction of persistence diagrams, where no specific information about individual path connected components is retained (see Section 3 for more details). Moreover, Definition 3 does not require any additional structure for the space X . Other choices are possible; for instance, if $X = \mathbb{R}$ the path connected components of f could be given a natural ordering.

2.5 Height and Weight Functions

A final step is needed to complete the construction of the merge trees we are going to use in the following sections. The height function h_T of a tree T takes values in \mathbb{R} , but this is not an *editable* space, as defined in [\[Paper Metriche\]](#). Hence we transform the height function h_T into a weight function w_T defined on V_T and such that the image of $V_T - \{r_T\}$ is a subset of the editable space $\mathbb{R}_{\geq 0}$.

For every vertex $v \in V_T - \{r_T\}$, we consider the unique edge between v and its father w and we define $w_T(v) = h_T(w) - h_T(v)$. We set $w_T(r_T) = h_T(r_T)$. Note that there is a one-to-one correspondence between h_T and w_T . Finally, the monotonicity of h_T guarantees that $w_T(v) \in \mathbb{R}_{\geq 0}$, for all $v \in V_T - \{r_T\}$.

The height function introduced in Definition 2 turns out to be quite natural for the definition of a merge tree, but from now on we replace the height function h_T with the induced weight functions w_T .

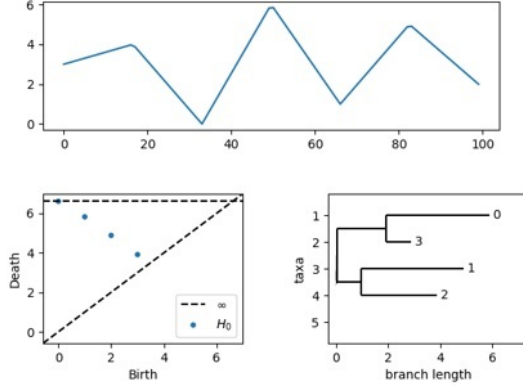


Figure 2: A function with its associated persistence diagram (left) and merge tree (right). On the PD axes we see the birth and death coordinates of its points. The plot of the merge tree features the length of its branches (given by the weight function) on the horizontal axis, and the leaves (taxa) are displaced on the vertical axis. The vertical axis scale is only for visualization purposes.

3. Persistence Diagrams

Persistence diagrams are arguably among the most well known tools of TDA; for a detailed survey see, for instance, (Edelsbrunner and Harer, 2008). We here briefly introduce them since in the following sections we use them to draw comparisons with merge trees.

Loosely speaking a persistence diagram is a collection of points (c_x, c_y) in the first quadrant of \mathbb{R}^2 , with $c_y > c_x$ and such that: c_x is the t corresponding to the first appearance of an homology class in X_t (birth), while c_y is the t where the same class merges with a different class appeared before c_x (death). Homology classes are a generalization of path-connected components to “holes in higher dimension”. For more details see Hatcher (2000).

In this work we focus on persistence diagrams associated to path-connected components, since we want to compare them with the merge trees introduced in the previous section. Given a function $f : X \rightarrow \mathbb{R}$, we associate to f the zero dimensional persistence diagram ($PD(f)$) of the sequence of sublevel sets $\{X_t\}_{t \in \mathbb{R}}$. In such representation there is no information about which path-connected component merges with which; in fact a component represented by the point (c_x, c_y) , at height c_y could merge with any of the earlier born and still alive components. Of course this collection of points depends on the shape of the function and in particular depends on its amplitude and the number of its oscillations. See Figure 2. Note that, while for merge trees one needs to be careful and consider appropriate isomorphism classes so that the representation does not depend on, for instance, the names chosen for the vertices (that is, the set V_T), this issue does not appear with persistence diagrams. Topological features are represented as points in the plane, without labels or other kinds of set-dependent information. Thus, two persistence diagrams are isomorphic if and only if they are made of the same set of points.

4. Properties

In this section we state the main invariance result anticipated in the introduction and we also point out a few differences between persistence diagrams and merge trees.

Proposition 1 (Invariance) *The (isomorphism class of the) merge tree and the persistence diagram of the function $f : X \rightarrow \mathbb{R}$, are both invariant under homeomorphic re-parametrization of f .*

Remark 1 *As an immediate consequence of Proposition 1 we obtain that, if the functions f and g can be aligned by means of an homeomorphism, that is if $f = g \circ \eta$ being η an homeomorphism, then their associated merge trees T_f and T_g are isomorphic and the same holds for $PD(f)$ and $PD(g)$.*

In other words, we can warp, deform, move the domain X of a function f by means of any homeomorphism, and this will have no effect on its associated PD or merge tree. As a consequence, if each element of a sample of functions is represented by its merge tree, or by its persistence diagram, one can carry out the statistical analysis without worrying about possible misalignment, that is without first singling out, for each function of the sample, the specific warping function, identified by an homeomorphism, which decouples its phase and amplitude variabilities.

Despite sharing this important invariance property, a persistence diagram and a merge tree are not equivalent representations of a function. Indeed, persistence diagrams do not record information about the merging components. This is an important difference, since merge trees can capture also this local structure of a function (see Figure 3). Moreover, the next proposition proves that the information contained in the persistence diagram of a function f can be retrieved from the merge tree associated to f , but the converse is not true as shown in Figure 3

Proposition 2 *For all $f : X \rightarrow \mathbb{R}$, the associated $PD(f)$ can be obtained by the associated merge tree T_f .*

Thus, if two functions induce isomorphic merge trees, they also have the same persistence diagrams.

5. Metrics

We want to analyze sets of functions using merge trees and PDs, exploiting metrics which have already been defined respectively in [\[Paper Metriche\]](#) and in Cohen-Steiner et al. (2010). Here we quickly present such metrics, with a special focus on the metric for merge trees, since we use it to develop novel stability results in the next sections.

5.1 Metrics for Persistence Diagrams

The space of persistence diagrams can be given a metric structure by means of a family of metrics which derives from Wasserstein distances for bivariate distributions.

Given two diagrams D_1 and D_2 , the expression of such metrics is the following:

$$W_p^p(D_1, D_2) = \inf_{\gamma} \sum ||x - \gamma(x)||_{\infty}^p$$

where γ are functions partially matching points between diagrams D_1 and D_2 , and matching remaining points with the line $y = x$ on the plane. In other words we measure the distances between the points of the two diagrams, pairing each point of a diagram either with a point on the other diagram, or with a point on $y = x$. Each point can be matched once and only once. The minimal cost of such matching provides the distance.

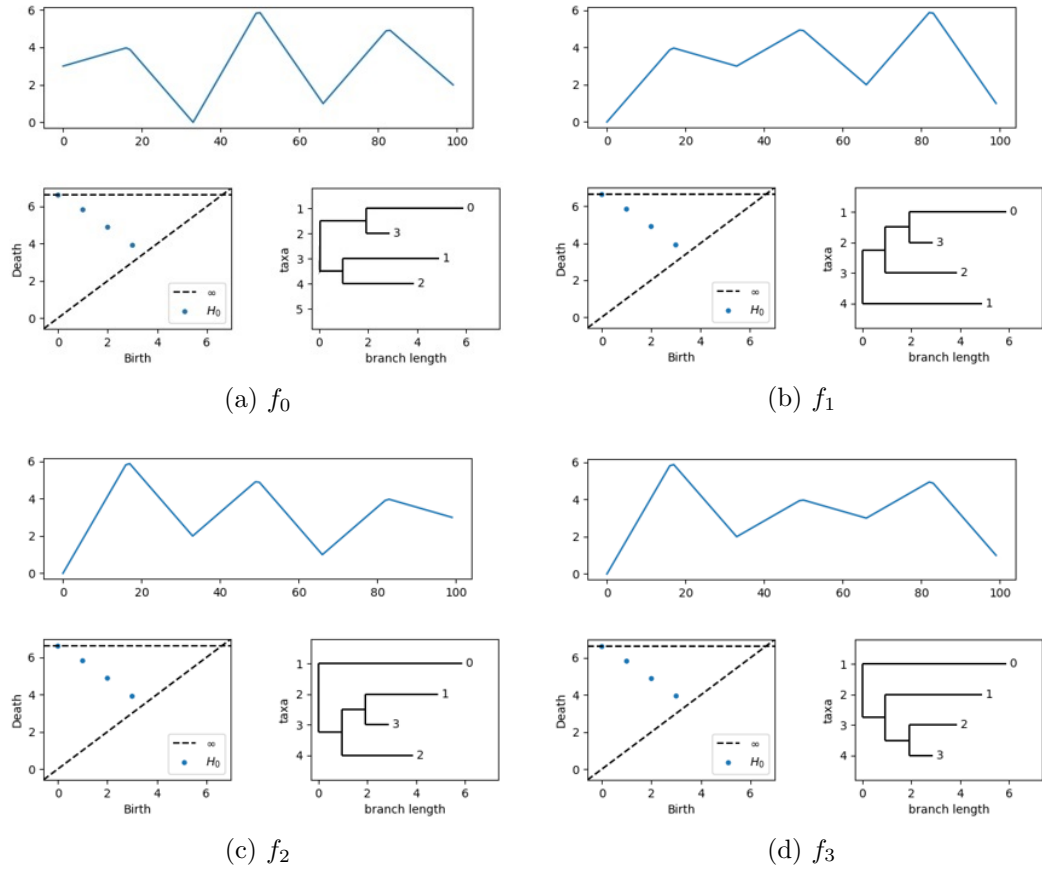


Figure 3: We compare four functions; they are all associated to the same PD but to different merge trees. Functions are displayed in the first row of each subplot, while on the second we have on the left the associated PD and on the right the merge tree.

5.2 Metric for Merge Trees

The metric for tree-like objects defined in [Paper Metriche] is based on edit distances (Bille, 2005; Hong et al., 2017): they allow for modifications of a starting object, each with its own cost, to obtain a second object. Merge trees equipped with their weight function w_T , as defined in Section 2.5, fit into this framework; hence the space of merge trees can be endowed with a metric based on an edit distance and called d_E in the following.

The distance d_E is very different from previously defined edit distances, since it is specifically designed for comparing topological summaries. It satisfies the property of *topological stability* (see Section 5.2.1), roughly meaning that all points which are topologically irrelevant can be eliminated by a merge tree without paying any cost. To make things more formal we here introduce the edits, as defined in [Paper Metriche], but directly in the context of merge trees, since they were originally defined for more general objects.

The edits are the followings:

- *shrinking* an edge means changing the weight value of the edge with a new positive value. The inverse of this transformation is the shrinking which restores the original edge weight.
- *deleting* an edge (v_1, v_2) results into a new tree, with the same vertices apart from v_1 (the lower one), and with the father of the deleted vertex which gains all of its children. This edit cannot be done on the root. With a slight abuse of language, we might also refer to this edit as the deletion of the vertex v_1 , which indeed means deleting the edge between v_1 and its father.

The inverse of deletion is the *insertion* of an edge along with its child vertex. We can insert an edge at a vertex v specifying the child of v and its children (that can be either none or any portion of the children of v) and the weight of the edge.

- Lastly, we can eliminate an order two vertex v , that is a father with an only child, connecting the two adjacent edges which arrive and depart from v . The weight of the resulting edge is the sum of the weights of the joined edges. This transformation is the *ghosting* of the vertex v and it cannot be done on the root. Its inverse transformation is called the *splitting* of an edge.

Remark 2 *Edit operations are not globally defined as operators mapping merge trees into merge trees. They are defined on the individual tree. Similarly, their inverse is not the inverse in the sense of operators, but it indicates that any time we travel from a tree T to a tree T' by making a sequence of edits, we can also travel the inverse path going from T' to T and restore the original tree.*

The costs of the edit operations are defined as follows:

- the cost of shrinking an edge is equal to the absolute value of the difference of the two weights;
- for any deletion/insertion, the cost is equal to the weight of the edge deleted/inserted;
- the cost of ghosting is zero.

The root of a merge tree can only be edited by changing its weight and the cost of such editing is the absolute value of the weight change.

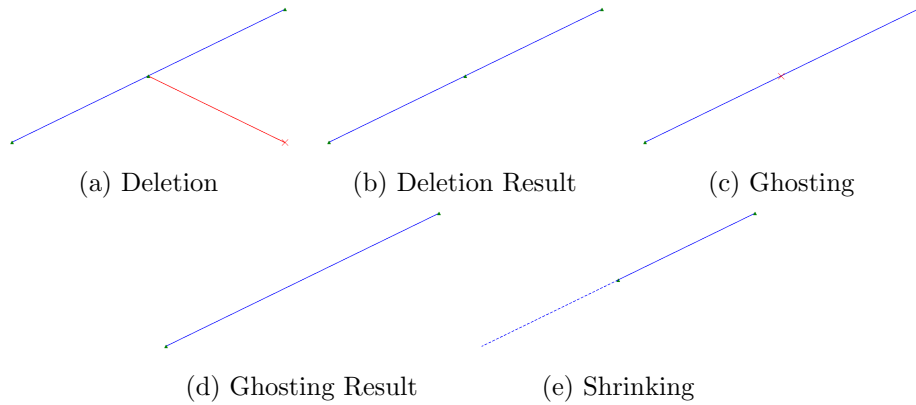


Figure 4: (a)→(e) form an edit path made by one deletion , one ghosting and a final shrinking.

Given a tree T we can edit it, thus obtaining another tree, on which we can apply a new edit to obtain a third tree and so on. Any finite composition of edits is called *edit path*. The cost of an edit path is the sum of the costs of its edit operations. Putting all the pieces together, we can define the edit distance d_E as:

$$d_E(T, T') = \inf_{\gamma \in \Gamma(T, T')} \text{cost}(\gamma)$$

where $\Gamma(T, T')$ indicates the set of edit paths which start in T and end in T' .

5.2.1 ORDER TWO VERTICES

The null cost of ghosting guarantees that order 2 vertices are completely irrelevant when computing the cost of an edit path.

Definition 5 *If there is an edit path from the tree T to the tree T' consisting only of ghosting edits, we say that the two trees are equal up to order 2 vertices. By definition, the length of the edit path starting in T and ending in T' is equal to 0.*

In [Paper Metriche] it is proved that d_E is a metric on the space of merge trees, identified up to order 2 vertices. As explained in [Paper Metriche], the fact that order 2 vertices are irrelevant is precisely what makes the metric d_E suitable for comparing merge trees and is fundamental to obtain the results of the following Section 6.

6. Pruning & Stability

As stated in the introduction of the paper, any time we use a data representation – or we further transform a representation – it is important to understand and explore the properties of the operators involved. In particular, in this section we establish some continuity properties for the operator $f \mapsto T_f$, which maps a function to its merge tree. Conditional on the topology endowing the functional space where the function f is embedded, these properties dictate how the variability between functions is captured by the variability between their merge tree representations.

Proposition 1 implies that the merge tree representation of a function f is unaffected by a large class of warpings of its domain, which would strongly perturb f if it was embedded, for instance, in an L_p space, with $p \neq \infty$. As an example, if $f : \mathbb{R} \rightarrow \mathbb{R}$ has compact support, shrinking f by setting $f_n(x) = f(x \cdot \lambda_n)$ with $\lambda_n \rightarrow +\infty$, produces no

effect on the merge tree representation of f since $T_{f_n} = T_f$, while the p -norm of f_n goes to zero.

It might therefore be more natural to study the behavior of $f \mapsto T_f$ endowing the space of functions $f : X \rightarrow \mathbb{R}$ with the topology of pointwise convergence, which captures pointwise closeness between functions. This topology, available for any domain X , has also the advantage of showing the effect of pointwise noise on merge tree representations.

6.1 Pruning

We know that, given f , the merge tree T_f will mostly depend on the critical points of f : as the number of spikes of f grows, also the size of the tree grows, while the weights of its branches grow with the height of the spikes. Similarly, if two functions $f, g : X \rightarrow \mathbb{R}$ are pointwise ε close, we can say that the shape of the functions is the same up to spikes of height $2 \cdot \varepsilon$. Each such spike would cause the birth of a leaf whose branch is shorter than $2 \cdot \varepsilon$; the trees must therefore be the same up to branches of weight $2 \cdot \varepsilon$. These considerations move the idea of pruning, which consists of removing unessential edges from a tree.

Given a merge tree without order 2 vertices, we delete the small weight leaves, that is those whose weight is smaller than or equal to a given fixed threshold. However, if two or more small weight leaves are siblings, we only remove that of smallest weight, or one of the leaves chosen at random if they have the same weight, and then ghost its father if it becomes an order 2 vertex. This procedure is done recursively until no small weight leaves are found. Note that removing only one leaf in case of siblings of small weight, prevents the possible removal of information relative to spikes of f with amplitude larger than the threshold.

We can thus define the pruning operator:

$$P_\varepsilon : \mathcal{T} \rightarrow \mathcal{T}$$

such that $P_\varepsilon(T)$ is the tree obtained by pruning with threshold ε . Notice that P_ε is idempotent, that is $P_\varepsilon(P_\varepsilon(T)) = P_\varepsilon(T)$.

Remark 3 P_ε is not a continuous operator. Consider T formed by just one edge with weight ε ; take $\delta > 0$ and consider T' , with the same tree topology as T but made by one edge of weight $\varepsilon + \delta$. Now, $d_E(T, T') = \delta$ and $d_E(P_\varepsilon(T), P_\varepsilon(T')) = \varepsilon + \delta$. If we let $\delta \rightarrow 0$, then $d_E(P_\varepsilon(T), P_\varepsilon(T')) > \varepsilon$.

For what has been said up to now, the operator P_ε can be considered as a smoothing operator. We fix some threshold which we think captures meaningful shape changes in a function and then, consistently, we remove what is deemed to be noise from the representation, obtaining a more regular merge tree. This has also the effect of greatly decreasing the number of leaves of the tree, a fact that is important from the computational perspective.

6.2 Stability

Now we study the case of two merge trees T_f and T_g representing functions f and g which are pointwise ε close.

The main theorem of this section is the following.

Theorem 1 Let f, g be tame functions defined on a path connected topological space X and such that

$$\sup_{x \in X} |f(x) - g(x)| \leq \varepsilon.$$

Let T_f and T_g be the merge trees associated to f and g respectively and let N and M be the cardinalities of V_{T_f} and V_{T_g} .

Then, there exists an edit path $e_1 \circ \dots \circ e_{N \cdot M} \in \Gamma(T_f, T_g)$ such that $\text{cost}(e_i) < 2 \cdot \varepsilon$, for $i = 1, \dots, N \cdot M$.

Theorem 1 states that if two functions are pointwise close, then we can turn the merge tree associated to the first function into the merge tree associated to the second function, using edits of small cost, at most one per vertex. Note, however, that if the two functions have a very high number of oscillations, the distance between their merge trees could still be large. Indeed if $\|f_n - f\|_\infty \xrightarrow{n} 0$ with $\#V_{T_{f_n}} \xrightarrow{n} \infty$, we are not guaranteed that $d_E(T_f, T_{f_n}) \rightarrow 0$. Theorem 1 however implies that, if the cardinalities $|V_{T_{f_n}}|$ are bounded, then $d_E(T_f, T_{f_n})$ indeed converges to 0.

Problems could then arise when we expect a possibly unbound number of informative spikes, that is spikes which should not be removed by pruning. In this case, however, the computational cost of the metric d_E would also be prohibitive due to the high number of leaves in the trees; indeed this supports the claim that the only practical limitation to the use of the metric d_E is given by its computational cost.

6.3 Spline Spaces

We here emphasize for spline spaces the consequences of the results of the previous two subsections, since splines are often used in FDA applications for smoothing the discrete raw data profiling each statistical unit in the sample.

As already noted in the introduction, spline spaces are a preferred tool for smoothing functional data since they provide finite dimensional vector spaces of functions with convenient properties. In particular, spline functions are piecewise polynomials determined by a grid of knots; fixing the knots determines a finite upper bound for the number of critical points of the spline. Consider for instance \mathcal{S}_n^3 , the space of piecewise cubic polynomials over a grid on $[0, 1]$ with n equispaced knots. On each interval the first derivative of the function is a quadratic polynomial and thus its zero set is composed by at most two points. This means that the number of critical points of $f \in \mathcal{S}_n^3$ is at most $2(n - 1)$; therefore the number of leaves of the tree T_f associated to f cannot be greater than $2(n - 1)$. The following Corollary of Theorem 1 is in fact easily obtained:

Corollary 1 *Let \mathcal{S} be a space of piecewise polynomial functions of some fixed degree, all defined by means of the same finite grid of nodes. Then the operator $f \in \mathcal{S} \mapsto T_f$ is continuous.*

Smoothing raw data with splines entails a delicate trade-off between being flexible, to capture the salient features of the function the raw data have been sampled from, and avoiding the introduction of artifacts, due, for instance, to noise overfitting or caused by forcing the spline to fit an abrupt spike. Representing the smoothed spline function by means of a merge tree can help in handling this trade-off, by allowing the analyst a certain degree of casualness in the smoothing phase, since the small artifacts generated by a possible overfitting will then be controlled by pruning the tree.

For instance, consider the problem of approximating $f : [0, 1] \rightarrow \mathbb{R}$ with a cubic spline function defined by an equispaced grid of knots. Suppose f satisfies some regularity conditions, usually implied by its embedding in a Sobolev space. The parameter which controls the bias-variance trade-off is just the number of knots n . Many results are known in the literature concerning the uniform convergence of spline functions as the step of

the grid of knots goes to zero (see for instance De Boor and Daniel (1974)) and most of them are given in terms of a factor $1/n^\alpha$ and the norm of the derivatives or the modulus of continuity of f . In other words, the pointwise error can be reduced as needed by increasing n . When f is approximated by the spline function s_f with an error of ε in terms of uniform norm, this means that whatever happens in intervals of $\pm\varepsilon$ around f is inessential. Stated in different terms, oscillations of s_f taking place in such zone are to be considered uninformative with respect to the analysis. Thus a sensible choice is to represent the function f fitted by the spline s_f by means of the pruned merge tree $\mathcal{P}_{2\varepsilon}(T_{s_f})$. If ε is small enough with respect to the oscillations of f , Theorem 1 implies that pruning T_{s_f} by 2ε removes only inessential edges of s_f , without loosing important information about f .

The same argument applies when smoothing observations sampled from a function f . The analyst may allow the spline to overfit the data and then decide that oscillations under a certain amplitude are irrelevant, controlling them by pruning the merge tree associated to the fitted spline.

7. Visualization trick

Before showcasing the examples and a case study, we point out a *visualization trick* employed when we graphically represent merge trees for visual comparison and evaluation.

Given a set of functions, each represented by a merge tree, we let M be the maximum value attained by any function in the set, and to each representing tree, say T , we add an edge connecting its root r_T to a new point, which becomes the new root, at height M . The new edge of course is given weight $M - w_T(r_T)$. In this way all merge trees in the dataset are "hanging" from height M , and can therefore be visually compared using existing libraries for trees representation. See Figure 5.

Moreover, apply this visualization trick to two trees T_f and T_g . The cost of shrinking the edge of weight $M - w_{T_f}(r_{T_f})$ added to the tree T_f to the corresponding edge added to the tree T_g is exactly $|w_{T_f}(r_{T_f}) - w_{T_g}(r_{T_g})|$ and this is the cost of editing the roots r_{T_f} and r_{T_g} to match heights. Hence, the visual comparison of the merge tree representations is consistent with the metric d_E .

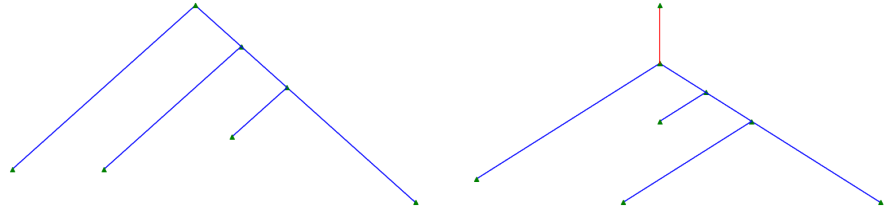
8. Examples

These examples are intended to show the differences between persistence diagrams and merge trees, already highlighted in Section 4.

8.1 Example I

We generate two clusters of functional data such that the membership of a function to one cluster or the other should depend on the amplitude of its oscillations and not on the merging structure of its path connected components. We then look at the matrices of pairwise distances between functions, comparing merge tree and persistence diagram representations in terms of their goodness in identifying the clustering structure.

To generate each cluster of functions, we draw, for each cluster, an independent sample of 16 critical points, 8 maxima and 8 minima, from two univariate Gaussian distributions with means equal to $+100$ for maxima and to -100 for minima, respectively. The standard deviations of the two Gaussian distributions are the same and they are set equal to 50. To generate a function inside a cluster, we draw a random permutation of 8 elements and according to that permutation we reorder both the set of maxima and the set of minima



(a) Tree structure T . Suppose (b) Tree structure T with the added
 $h_T(r_T) = 1$ and $M = 2$. edge of lenght 1 and the new root.

Figure 5: On the left we can partially see a merge tree: namely we see its tree structure with the weights represented by the length of the edges. The information about the height value of the root is not visualized. On the right we see the same merge tree represented with the visualization trick: the red edge allows a visual comparison between different merge trees represented in such way.

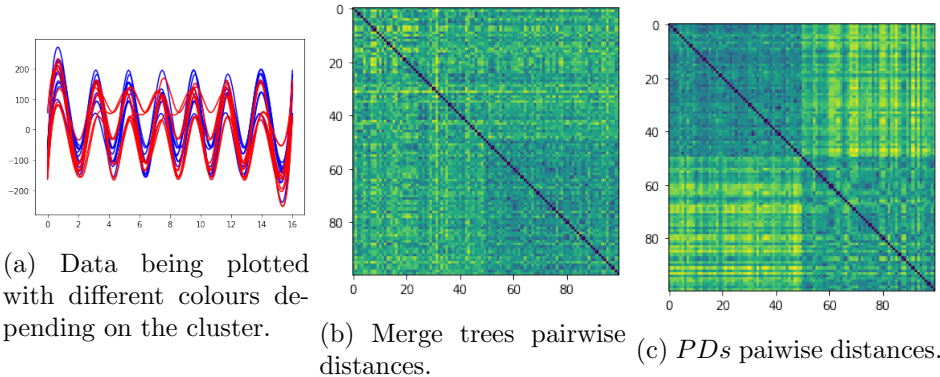


Figure 6: Example I. In the first row we can see few data from the two clusters. In the second row we see the matrices of pairwise distance extracted with trees and PDs . The data are ordered according to their cluster. It is clear how PDs perform much better in separating the two clusters.

associated to the cluster. Then, we take a regular grid of 16 nodes on the abscissa axis: on the ordinate axis we associate to the first point on the grid the first minimum, to the second the first maximum, to the third the second minimum and so on. To obtain a function we interpolate such points with a cubic spline. We thus generate 50 functions in each cluster. The key point is that, within the same cluster, the critical points are the same but for their order, while the two clusters correspond to two different sets of critical points.

In this example, we expect that the clustering structure carried by the amplitude of the functions will be shadowed by the differences in the merging order, when adopting the merge tree representation; while persistence diagrams should perform much better because they are less sensitive to peak reordering. This is in fact confirmed by inspecting the distance matrices in Figure 6b and Figure 6c.

8.2 Example II

Here we reverse the state of affairs and we set the feature for discriminating between clusters to be the merging structure of the functions. Hence, we generate two clusters of functions: the members of each cluster have the same merging structure which is however different between clusters.

To generate the two clusters of 50 functions each, we first draw an independent sample of 10 critical values, 10 maxima and 10 minima, shared between the clusters. Such samples are drawn from Gaussian distributions with means 100 and -100 respectively and standard deviation 200. Given a regular grid of 20 nodes on the abscissa axis, on the ordinate axis we associate to the first point of the grid a maximum, to the second a minimum, and so on, as is Example I. To generate every member of one cluster or the other, we add to the ordinate of each maximum or minimum critical point a random noise generated by a Gaussian with mean 0 and standard deviation 100. Then we reorder such points following a cluster-specific order. And, lastly, we interpolate with a cubic spline. We remark that the ordering of the maxima and that of the minima now becomes essential. For the two clusters, these orderings are fixed but different and they are set as follows (0 indicates the smallest value and 9 being the largest value):

- first cluster: maxima are ordered along the sequence $(0, 1, 2, 3, 4, 5, 6, 7, 8, 9)$, minima along the sequence $(0, 1, 2, 3, 4, 5, 6, 7, 8, 9)$;
- second cluster: maxima are ordered along the sequence $(3, 2, 1, 0, 8, 9, 7, 6, 4, 5)$, minima along the sequence $(3, 2, 1, 0, 8, 9, 7, 6, 4, 5)$.

Such different orderings provide non-isomorphic tree structures for the merge trees associated to the functions of the two clusters, as we can see in Figure 8, while keeping a similar structure in terms of persistence diagrams.

In this example, we expect *PDs* to be unable to recognise the clustering structure among the data; indeed, the only discriminant feature available to *PDs* is the different height of critical points, but this bears little information about the clusters.

We can visually observe this by comparing Figure 7b with Figure 7c.

9. Case Study

We now run a comparative analysis of the real world Aneurisk65 dataset. This dataset – and the clinical problem for which it was generated and studied – was first described in Sangalli et al. (2009b), but it has since become a benchmark for the assessment of FDA methods aimed at the supervised or unsupervised classification of misaligned functional

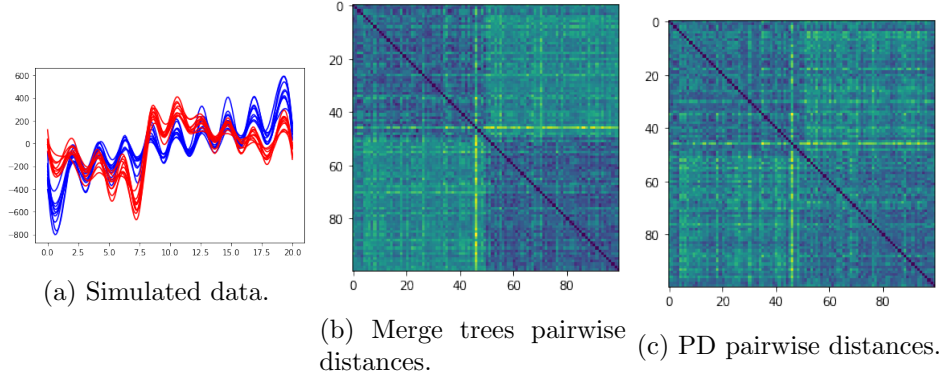


Figure 7: Example II. In the first row we can see a few data from the two clusters. In the second row we see the matrices of pairwise distances between merge tree representations and *PDs*, respectively. The data are ordered according to their cluster. It is clear how in this example merge trees are more suitable to separate the two clusters.

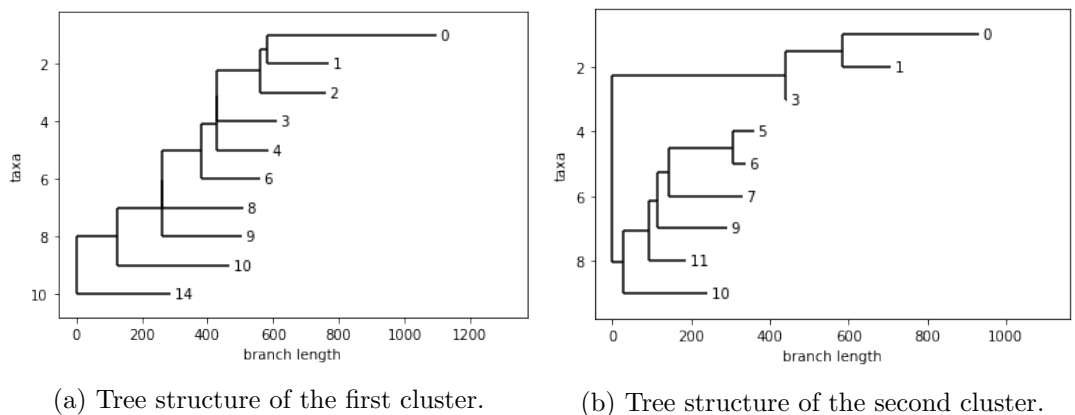


Figure 8: Example II. The tree structures of the two clusters.

data (see, for instance, the special issue of the Electronic Journal of Statistics dedicated to phase and amplitude variability - year 2014, volume 8). We then repeat the classification exercise illustrated in Sangalli et al. (2009b) with the double scope of comparing merge trees and persistent diagrams when used as representations of the Aneurisk65 misaligned functional data, and of evaluating the performance of these representations for classification purposes when compared with the results obtained with the more traditional FDA approach followed by Sangalli et al. (2009b).

9.1 Dataset

The data of the Aneurisk65 dataset were generated by the Aneurisk Project, a multi-disciplinary research aimed at investigating the role of vessel morphology, blood fluid dynamics, and biomechanical properties of the vascular wall, on the pathogenesis of cerebral aneurysms. The project gathered together researchers of different scientific fields, ranging from neurosurgery and neuroradiology to statistics, numerical analysis and bio-engineering. For a detailed description of the project scope and aims as well as the results it obtained see its web page (<https://statistics.mox.polimi.it/aneurisk>) and the list of publications cited therein.

Since the main aim of the project was to discover and study possible relationships between the morphology of the inner carotid artery (ICA) and the presence and location of cerebral aneurysms, a set of three-dimensional angiographic images was taken as part of an observational study involving 65 patients suspected of being affected by cerebral aneurysms and selected by the neuroradiologist of Ospedale Niguarda, Milano. These 3D images were then processed to produce 3D geometrical reconstructions of the inner carotid arteries for the 65 patients. In particular, these image reconstructions allowed to extract, for the observed ICA of each patient, its centerline “raw” curve, defined as the curve connecting the centres of the maximal spheres inscribed in the vessel, along with the values of the radius of such spheres. A detailed description of the pipeline followed to identify the vessel geometries expressed by the AneuRisk65 functional data can be found in Sangalli et al. (2014).

Different difficulties arise when dealing with this data. First, as detailed in Sangalli et al. (2009a), to properly capture information affecting the local hemodynamics of the vessels, the curvature of the centerline must be obtained in a sensible way. Retrieving the salient features of the centerline and of its derivatives is a delicate operation, which is heavily affected by measurement errors and reconstruction errors, due to the complex pipeline involved. Consequently the “raw” curves appear to be very wiggly and it is not obvious how to produce reasonable smooth representations. At the same time the 3D volume captured by the angiography varies from patient to patient. This is due to many factors, such as: the position of the head with respect to the instrument, which in turns depends on the suspected position of the aneurysm, the disposition of the vessels inside the head of the patient, the size of the patient. We can recognize these differences even by visual inspection in Figure 9: for instance, in Figure 9a and Figure 9g we see a longer portion of the ICA than in Figure 9d. Therefore the reconstructed ICAs cannot be directly compared: we need methods that take into account that the centerlines are not embedded in \mathbb{R}^3 in the same way, and that we cannot expect potentially interesting features to appear in exactly the same spots along the centerline. This is the typical situation where one should resort to alignment.

Hence, this dataset is paradigmatic of the three-faceted representation problem highlighted in the introduction; data smoothing, embedding, and alignment present difficult challenges, which propelled a number of original works in FDA.

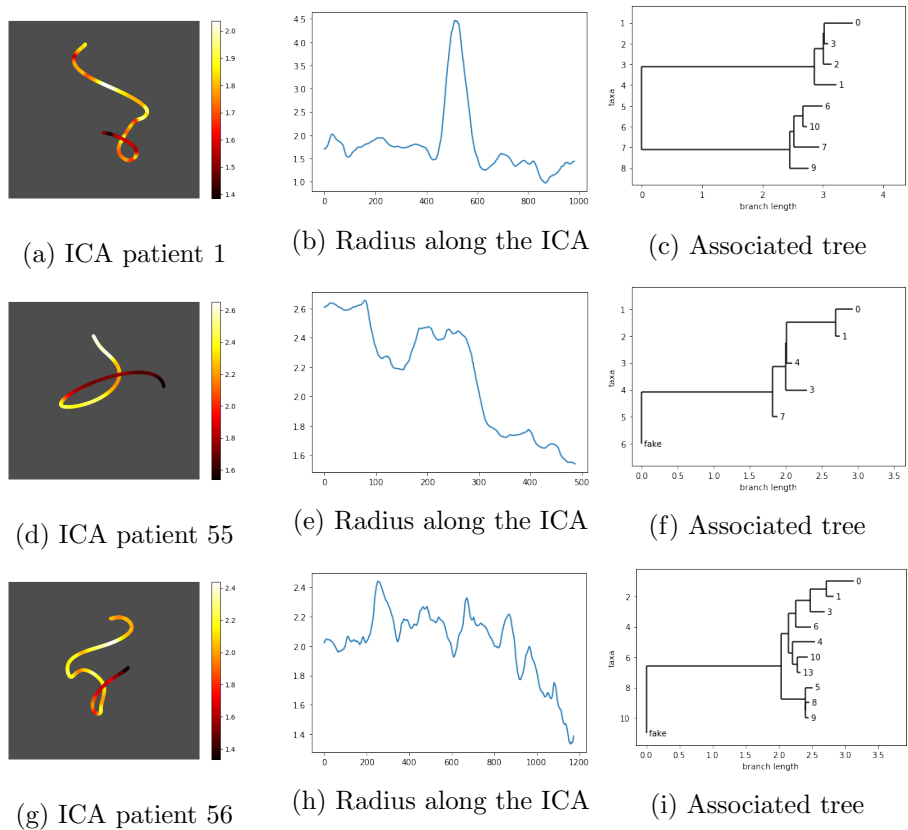


Figure 9: Three patients in the AneuRisk65 dataset; on the left column, ICAs are coloured according to the radius value, on the central column the radius functions, on the right column their associated merge trees. Patient 1 belongs to the Lower group, the other two patients to the Upper group.

The AneuRisk65 data have been already partially processed; in particular centerlines have been smoothed following the free-knot regression spline procedure described in Sangalli et al. (2009a), and their curvatures were thus obtained after computing the first two derivatives of the smoothed curves. The data relative to the radius of the blood vessel, instead, although measured on a very fine grid of points along the centerline, is still in its raw format. Hence the AneuRisk65 data also allow us to compare the behaviour of tree representations on smoothed data and on raw data.

9.2 Analysis

Patients represented in the AneuRisk65 dataset are organized in three groups: the Upper group (U) collects patients with an aneurysm in the Willis circle at or after the terminal bifurcation of the ICA, the Lower group (L) gathers patients with an aneurysm on the ICA before its terminal bifurcation, and finally the patients in the None group (N) do not have a cerebral aneurysm. Our main goal is supervised classification with the aim to develop a classifier able to discriminate membership to the group $L \cup N$ against membership to the group U based on the geometric features of the ICA. We complement this supervised analysis with an unsupervised exercise with the aim of clustering patients solely on the basis of the similarity of geometric features of their ICA, recovering a clear structure between the groups listed above and thus providing further support to the discriminating power of the geometric features of the ICA.

9.2.1 THE PIPELINE FOR SUPERVISED CLASSIFICATION

We develop a classification pipeline in close analogy with the one illustrated in Sangalli et al. (2009b) which, after smoothing, reduces the data dimensionality by means of Functional Principal Components Analysis (FPCA) applied to the curvature functions of the ICA centerlines and to the respective radius functions, and then fits a quadratic discriminant analysis (QDA) based on the first two FPCA scores of the curvature functions and of the radius functions respectively.

We interpolate the data points representing the smoothed curvature functions and the raw radius functions provided in the Aneurisk65 dataset with a piecewise linear spline and, for each patient, we consider the merge tree associated to its curvature and the merge tree associated to its radius. We then prune our tree representations; to use a uniform scale across all patients (but of course different for curvature and radius) we parametrize the pruning threshold as a fraction of the total range covered by the curvature and radius functions, respectively, across patients: $I = [\min_f(\min_x(f(x))), \max_f(\max_x(f(x)))]$. For both sets of trees, we then calculate the pairwise distances with the metric d_E and we organize them in two distance matrices. Blending the discriminatory information provided by curvature and radius, we also produce a new distance matrix collecting the pairwise distances obtained by convex linear combination of the distances for curvature and radius, according to the formula:

$$d_{\text{mixed}}^2 = w \cdot d_{\text{curvature}}^2 + (1 - w) \cdot d_{\text{radius}}^2, \quad (1)$$

where $0 \leq w \leq 1$. For lack of references, we prove in Appendix A.1 that d_{mixed} is a metric, for all $w \in [0, 1]$. We then apply Multi Dimensional Scaling (MDS) to each of the above distance matrices, to map the results in a finite dimensional Euclidean space of dimension m . Lastly, and following Sangalli et al. (2009b), we fit a QDA on such embedded points.

This pipeline requires the setting of three hyperparameters: the pruning threshold, the weight w appearing in Equation (1) and, finally, the dimension m of the Euclidean

embedding for MDS. While the pruning threshold is chosen with an elbow analysis, see Section 9.2.2, the weight w and the dimension m of the multidimensional scaling are selected by maximising the discriminatory power of QDA estimated by means of leave-one-out (L1out) cross-validation.

9.2.2 PRUNING

In this section, we take a closer look at the smoothing carried out by pruning the merge trees representations of curvature and radius. From the plots in Figure 9 we see that the radius functions appear to be very wiggly and, given the complex data-generating pipeline, we might assume that some portion of that amplitude variability is uninformative and due to different kinds of errors, which is the same conclusion drawn by Sangalli et al. (2009a) with respect to the raw curvature data. As detailed in Section 6.1, removing those little spikes from functions amounts to removing little branches from trees (up to smaller siblings). Thus, the number of leaves in a pruned tree is a monotone decreasing function of the pruning threshold: as the parameter grows, the number of leaves decreases.

We expect to find some separation in terms of amplitude between the proper features of the analyzed functions and the unwanted, “noisy” ones. Otherwise it would mean that the signal-to-noise ratio is so low that the uninformative errors shadow the informative features of the functions, and thus that the data are hopelessly corrupted. For this reason, we choose the pruning parameter through an elbow analysis of the curve plotting the number of leaves of the pruned trees, averaged over the whole dataset, against the corresponding threshold. Thus, we look for an elbow in the curves depicted in Figure 11.

We want here to emphasise the different behaviours of the curvature trees and of the radius trees. There is no clear elbow in Figure 11a, showing that there is no reason to believe that data show a large number of small uninformative noisy oscillations. This is not surprising because the curvature functions of the Aneursik65 dataset are the result of a very careful smoothing process. The curve in Figure 11b, related to radius, has instead a clear elbow structure (between 1% and 2%) in accordance with our expectations. Thus, we choose 2% as pruning threshold for the radius curves, whilst we do not prune curvature trees. We later discuss the robustness of our results with respect to these choices.

9.2.3 CLASSIFICATION RESULTS

We compare our classification results with those illustrated Sangalli et al. (2009b). The goal is the same: separating the class U from the classes L and N.

Table 1 reports the prediction errors obtained after L1out cross-validation. As in Sangalli et al. (2009b), we obtain the best classifier by simultaneously considering the combined information conveyed by the couple of curvature and radius functions; the dissimilarity between different couples is measured by the distance in Equation (1), where the parameter $w = 0.46$, being this the value which minimizes prediction error computed by L1out.

The same pipeline is followed when curvature and radius functions are represented by merge trees or by persistence diagrams. In the case of PDs’, we first removed the points (that is, the topological features) with persistence lower than a certain threshold (where the persistence is $c_y - c_x$, according to the notation used in Section 3). The threshold has been taken equal to the pruning parameter of the merge trees.

The first two rows in Table 1 compare prediction errors when merge trees or PD representations are used. From left to right, the table shows the L1out confusion matrices when distances between curvatures, radii or their joint couple are respectively considered.

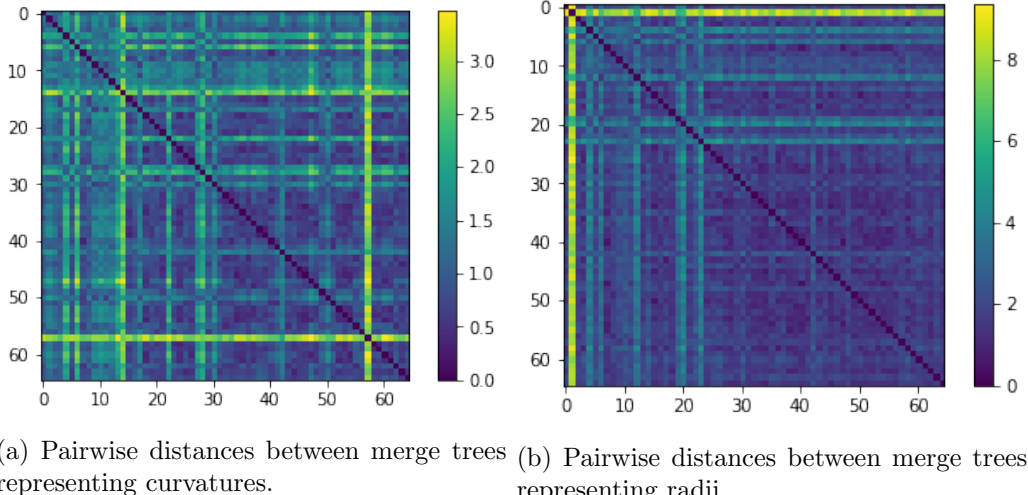


Figure 10: The distance matrices of merge trees associated to curvature and radius functions. Patients belonging to group L appear in first rows, followed by patients in the N group and patients in the U group.

We see that PDs do a better job in extracting useful information from either curvature or radius, when examined separately. This could be due to a situation not dissimilar from that illustrated in the example of Section 8.1: the discriminant information contained in the curvature and radius functions lies more in the number and amplitude of oscillations than in their ordering. However, when curvature and radius of the ICA are jointly considered as descriptors and the distance of Equation (1) is used, we obtain a better classifier for merge trees while there is no improvement for PDs.

This situation highlights that merge trees and persistence diagrams capture different pieces of information about the represented functions; moreover, PDs suggest that most of the information they capture is due to the radius function, while merge trees clearly show some informative interactions between curvature and radius.

For comparison, the third column of Table 1 reports the prediction errors of the best classifiers based on merge trees and on PDs, respectively, while the last row shows the prediction errors of the classifier described in Sangalli et al. (2009b). Although the number of patients misclassified by the best classifier based on merge trees is smaller than that of the best classifier based on PDs, we stress once again that the two methods are capturing different discriminant information; indeed, comparing the two analysis we found that only 6 patients were misclassified by both methods.

9.2.4 ROBUSTNESS WITH RESPECT TO THE PRUNING THRESHOLD

To argument in favor of the robustness of our results with respect to the choice of the pruning threshold, or, from another point of view, in favor of the robustness of the information conveyed by our tree representations of functions, we go through the same classification pipeline varying the value of the pruning threshold. In Figure 12 we show the prediction accuracy, estimated by L1out cross-validation, as a function of the pruning threshold. We notice that the accuracy is quite stable and, in particular for merge trees, slowly decreases as the threshold increases. This fact, on one hand further supports the elbow analysis approach described in Section 9.2.2, on the other is also showing that the results obtained

with the information captured by merge trees and persistence diagrams does not depend on a finely tuned choice of the threshold parameters.

9.2.5 CLUSTERING

We now explore the Aneurisk65 data clustering structure by endowing the merge tree space with the metric d_{mixed} figuring in Equation (1), with $w = 0.46$. To get multiple perspectives on this issue, we resort to hierarchical clustering dendrograms with different linkages. The visual inspection of Figure 10 suggests that, upon blending together the information of radius and curvature, the Upper class should display a low variability while the Lower and None classes should behave more heterogeneously. Thus, a clear clustering structure should not be recognizable: we expect possibly one cluster made by points belonging to the Upper class and then a series of points scattered around this central nucleus with no easily recognizable pattern.

The hierarchical dendrograms obtained with single, average and complete linkages are displayed in Figure 13. The first obvious observation is that all three linkages identify the point associated to patient 2 as an outlier. The single linkage dendrogram shows that, as the height on the dendrogram increases, there is only one major cluster which slowly becomes larger and incorporates all points in the data set. No other relevant clusters are found. Average and complete linkages further support this finding: there are no obvious heights where to cut the tree in the average linkage dendrogram; complete linkage instead shows perhaps a two cluster (plus one outlier) structure. The smaller cluster identified by this dendrogram, is also visible with the average linkage and is contained within the group of singletons obtained by cutting the single linkage tree at height 1.3. The overall picture is thus that of a major cluster, with possibly another group of points clustered together, but with much higher heterogeneity.

These findings can indeed be related with the labels declaring membership of the patients to the U , the N and the L group respectively. To grasp if there is an overall pattern in the merging structure of the data point cloud, for each leaf (a patient) of a dendrogram, we collect its merging height defined as the height of its father in the graph, that is the height at which that point is no longer considered as a singleton but instead it is clustered with some other point. In other words, we record the distance between the leaf and the closest cluster in terms of the cophenetic distance induced by the dendrogram. Note that, for the single linkage dendrogram, this is equivalent, for almost all leaves, to the height at which the leaf is merged with the major cluster. Results are shown in Figure 14. The interpretation of these plots is consistent across the different linkages and is pretty straightforward: the points corresponding to patients of the Upper group get merged within a small range of heights, and the distribution of their merging height is stochastically smaller than the distributions for groups L and N , respectively. The merging heights of the leaves corresponding to patients belonging to the Lower group, instead, display a larger variability and their distribution is stochastically larger than those of the leaves belonging to the other two groups. Patients of the class None, merge at heights in between the Upper and the Lower groups and their merging height seems to display a low variability. The plot (d) of Figure 14 shows the smoothed densities of the distributions of merging height for leaves belonging to the three groups, in the case of average linkage. Analogous representations could be obtained for the other two linkages; they all confirm the stochastic ordering described above.

This cluster analysis is consistent with our expectations, which, in turn, are in accordance to the findings of Sangalli et al. (2009b). On top of that, we also get two further insights: first, data are scattered around the Upper group with a possibly non uniform

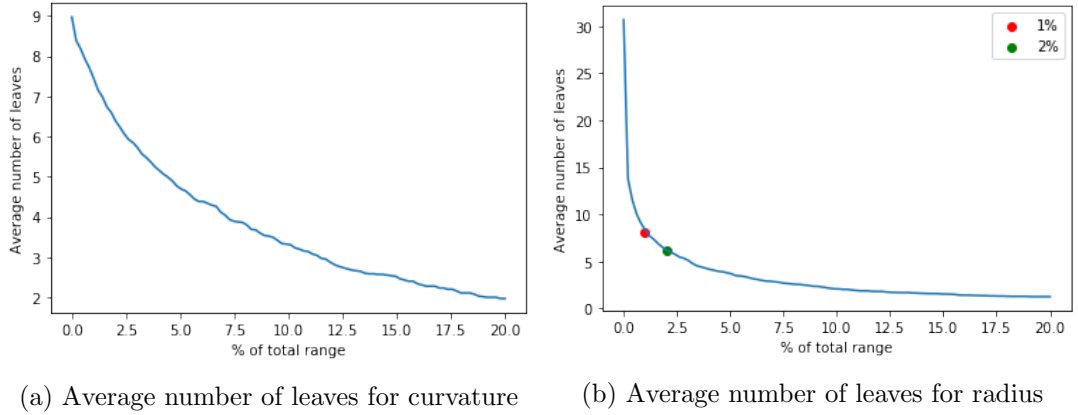


Figure 11: The average numbers of leaves in the merge trees, plotted against the percentage of total range used as pruning threshold.

Merge Trees		
Predicted		
Curvature		
True	U	L \cup N
	U	22
	L \cup N	7
	$w = 1, n = 3$	
Radius		
	U	16
	L \cup N	2
	$w = 0, n = 3$	
Mixed		
	U	25
	L \cup N	3
	$w = 0.46, n = 9$	

Persistence Diagrams		
Predicted		
Curvature		
True	U	L \cup N
	U	21
	L \cup N	3
	$w = 1, n = 3$	
Radius		
	U	26
	L \cup N	6
	$w = 0, n = 9$	
Mixed		
	U	26
	L	6
	$w = 0, n = 9$	

Benchmark		
Predicted		
True		
	U	L \cup N
	U	26
	L \cup N	6
	$w = 0, n = 9$	

Table 1: Confusion matrices for L1out. Below each confusion matrix, the values of the metric coefficient w and of the dimension m for MDS corresponding to the tested classifier are reported. The first row refers to the classifiers receiving as input merge tree representations, the second row PDs. The last row reports the benchmark L1out confusion matrix for the classifier illustrated in Sangalli et al. (2009b).

structure, as shown by the small and sparse cluster of Lower class patients visible with complete linkage clustering and, second, that the None group of patients lies in a sort of in between situation in the space separating the two other groups of aneurysm-affected patients. This could also explain the good performance of QDA: a quadratic boundary is able to isolate the core of the Upper group of patients from the others, which lie mainly on one side of the quadratic discriminant function.

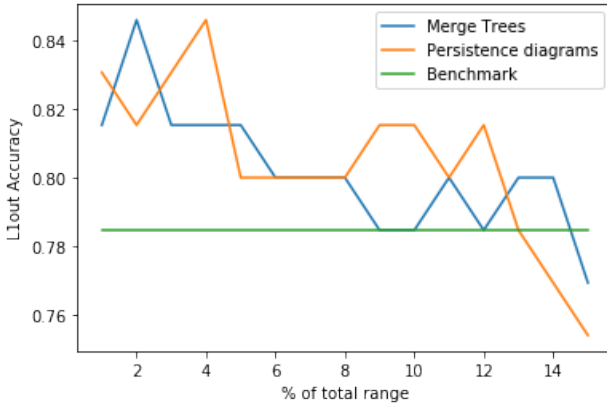


Figure 12: We can visually inspect robustness of the L1out accuracy of the classification pipeline - both for merge trees and persistence diagrams - with respect of the pruning threshold. The horizontal green line shows the accuracy obtained by Sangalli et al. (2009b). Note that the accuracy of persistence diagrams and merge trees is above or equal to the green line also for large values of the pruning threshold.

10. Discussion

We believe that methods from TDA can be fruitfully added to the toolbox of functional data analysis, especially when non trivial smoothing and alignment are required for data representation. In this paper we focused on two topological representations of functions: persistence diagrams, which, being the most classical tool in TDA, are regarded as a benchmark, and merge trees, which are rarely used in real data analysis applications. The framework for merge trees is the very recent metric structure defined in [\[Paper Metriche\]](#), for which we also developed theoretical results specific for the application to functional data.

To support our narrative, we used as paradigmatic real world application the classification analysis of the AneuRisk65 functional data set. This data set poses all the desired challenges: careful smoothing procedures and alignment techniques must be employed to obtain meaningful results. Reanalyzing the seminal case study described in Sangalli et al. (2009b), we show the advantages of having a representation of functional data which is invariant with respect to homeomorphic transformations of the abscissa – thus lightening the burden of careful alignment – and also allows for agile smoothing – possibly causing some overfitting – thanks to the pruning of the trees which takes care of this aspect of FDA which practitioners often find problematic. Following a classification approach based on QDA applied to proper reduced representations of the data, as in Sangalli et al. (2009b), we obtain robust results with comparable, if not better, accuracy in terms of L1out prediction error, and we confirm some facts about the variability of the data in the groups of patients characterized by the different location of the cerebral aneurysm, consistently with the findings of previous works.

To be sure, we want to stress that careful smoothing is still mandatory when precise differential information about the data is needed, since small oscillations in a function can still cause high amplitude oscillations in the derivatives, which cannot be removed by pruning. Moreover, not all FDA applications are adapted to the representations offered by merge trees or persistent diagrams. Indeed, the information collected by merge trees is contained in the ordering and in the amplitude of the extremal points of a function, and not on their exact abscissa. Hence, if the abscissa carries valuable information for

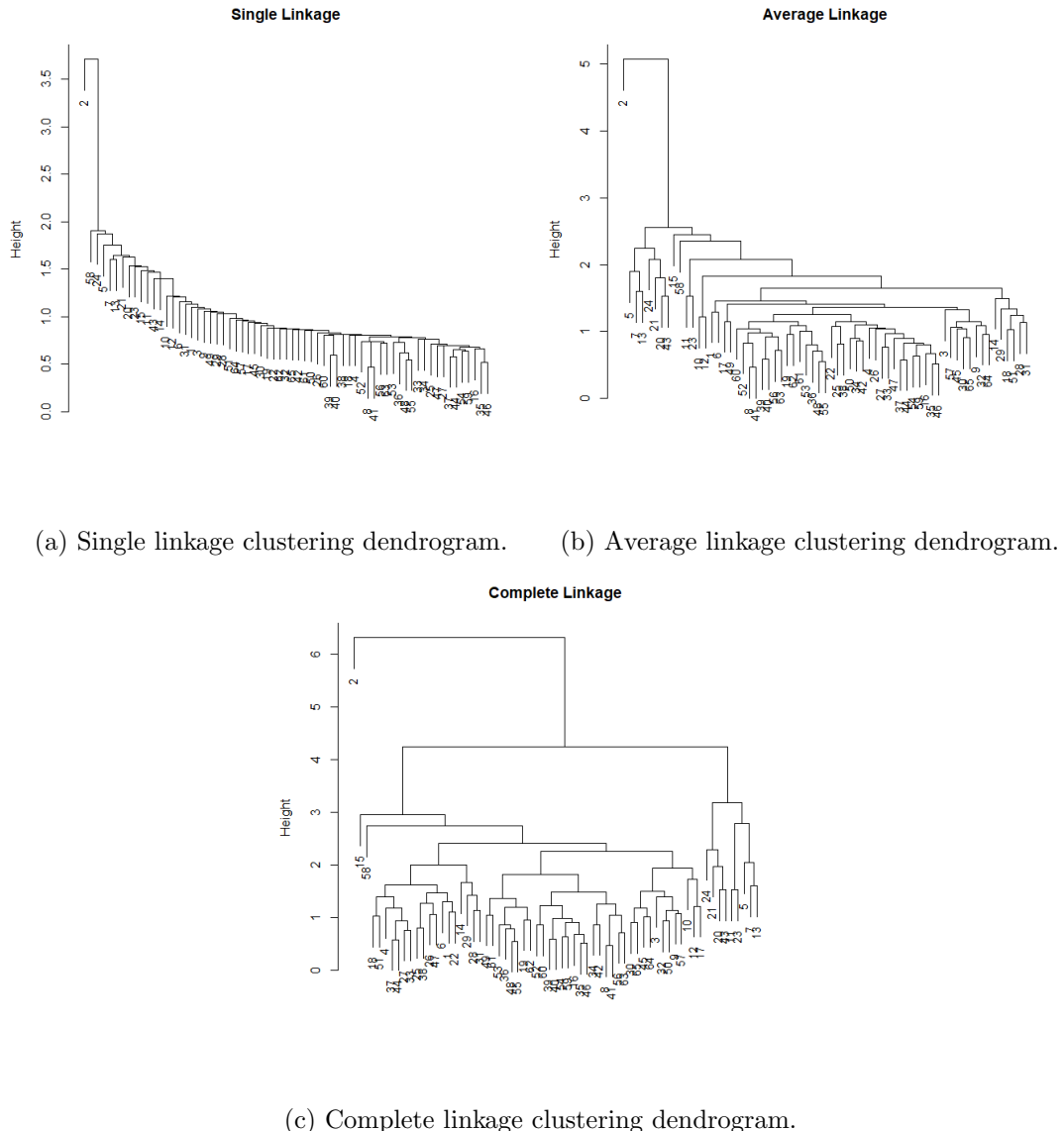
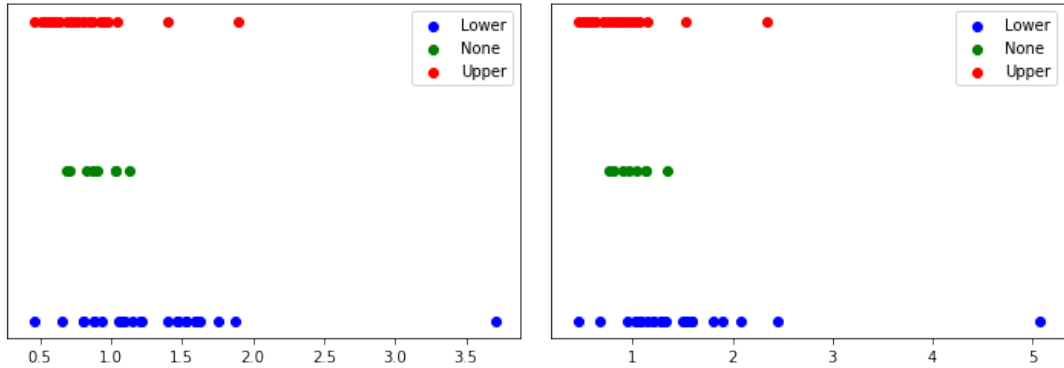
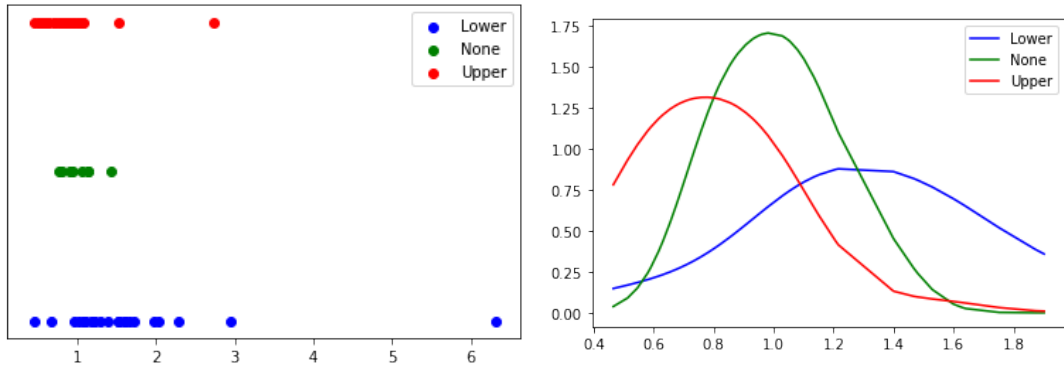


Figure 13: Hierarchical clustering dendrograms obtained with single, average and complete linkages.



(a) Heights at which leaves get merged in the single linkage clustering dendrogram. (b) Heights at which leaves get merged in the average linkage clustering dendrogram.



(c) Heights at which leaves get merged in the complete linkage clustering dendrogram. (d) Density estimate for the distributions in Figure 14b.

Figure 14: For each patient belonging to group U , L or N , the plots (a), (b) and (c) represent the merging height at which their corresponding leaf gets merged in the clustering dendograms, according to single linkage, average linkage and complete linkage, respectively. Plot (d) represents the smoothed densities of merging height for the leaves of the three groups, in the case of average linkage.

the analysis – for instance, a wavelength, or a precise landmark point in space or time – the TDA approach followed in this work for data representation is not indicated, precisely because of its invariance property with respect to homeomorphic transformations of the abscissa. But this criticism also applies to many alignment procedures proposed in the literature. Similarly, in Section 8.2 we point out that there are functions which have equivalent representations in terms of merge trees although the order on the abscissa of their critical points is different, although merge tree are much less sensitive to such issue when compared to persistence diagrams. If the order of critical points of the function is of importance for the analysis, then surely persistence diagrams, but possibly also merge trees, should be avoided.

Going general, we point out that whenever the datum designating a statistical unit is only a representative of an equivalence class, the analyst must be sure that the variability differentiating the members of the same class is ancillary with respect to the statistical analysis performed on the statistical units. This consideration always applies in FDA, whenever data are aligned according to transformations belonging to a group. Merge trees offer a representation of functional data in terms of equivalence classes whose members are invariant with respect to homeomorphic transformations of the abscissa. Persistence diagrams partition the space of functional data in even coarser equivalence classes, although they could be enough for the analysis, as we saw in the case study illustrated in Section 9. Occam’s razor should guide the analyst’s final choice.

11. Acknowledgements

We thank Steve Marron who initiated us to algebraic topology for the statistical analysis of functional data during seminal discussions while one of us (PS) was visiting him at UNC.

Appendix A. Proofs

Proof of Proposition 1.

Let $f : X \rightarrow \mathbb{R}$ be a bounded function defined on a path connected topological space X and let $\varphi : Y \rightarrow X$ be an homeomorphism. We need to prove that the merge tree and the persistence diagram associated to the function f and $f' = f \circ \varphi$ are isomorphic.

We know that:

$$Y_t = \{f'^{-1}((-\infty, t])\} = \{y | f'(y) \leq t\} = \{x = \varphi(y) | f(x) \leq t\}$$

This means that $y \in Y_t$ if and only if $\varphi(y) \in X_t$, and so $Y_t = \varphi^{-1}(X_t)$. In other words, φ maps sublevel sets into sublevel sets. Since the restriction of an homeomorphism is still an homeomorphism, it also sends connected components into connected components.

As a consequence $H_0(X_t) \simeq H_0(Y_t)$ and if $\{x_0, \dots, x_n\}$ is a basis made by connected components for $H_0(X_t)$ and $\{y_0, \dots, y_n\}$ for $H_0(Y_t)$, φ induces the following isomorphism of groups on the homologies: $\tilde{\varphi} : H_0(X_t) \rightarrow H_0(Y_t)$, such that $\tilde{\varphi}(x_i) = y_j$ for some j .

Given $t' < t$, we have the following commutative diagram:

$$\begin{array}{ccc} X_{t'} & \longrightarrow & X_t \\ \downarrow \varphi & & \downarrow \varphi \\ Y_{t'} & \longrightarrow & Y_t \end{array}$$

and passing to homologies:

$$\begin{array}{ccc} H_0(X_{t'}) & \xrightarrow{\alpha_X} & H_0(X_t) \\ \downarrow \tilde{\varphi} & & \downarrow \tilde{\varphi} \\ H_0(Y_{t'}) & \xrightarrow{\alpha_Y} & H_0(Y_t) \end{array}$$

where we remark that the φ 's are homeomorphisms and the $\tilde{\varphi}$'s are isomorphisms of groups.

The last diagram gives the isomorphism of $PD_0(f)$ and $PD_0(f')$.

Since connected components are sent to connected components (with both maps), this also becomes an isomorphism of merge trees: building the merge tree for Y_t and X_t would give isomorphic results. \blacksquare

Proof of Proposition 2.

Each leaf in T corresponds to a point in $PD(f)$. The x coordinate of each point is given by its height, which can be retrieved through h_f . Consider $v \in L_T$ and γ_v , the path from v to r_T which corresponds to the ordered set $\{v' \in V_T | v' \geq v\}$. The y coordinate of the points associated to v is the minimal height at which γ_v intersects γ_l , with l being a leaf with height less than v . \blacksquare

Proof of Theorem 1.

To prove the theorem, we need some notation and a couple of Lemmas.

Let f, g be tame functions on the path connected topological space X and such that $\sup_{x \in X} |f(x) - g(x)| \leq \varepsilon$. For $t \in \mathbb{R}$, we set $X_t^f = f^{-1}((-\infty, t])$. Since $|f(x) - g(x)| \leq \varepsilon$ we have $X_t^f \subset X_{t+\varepsilon}^g$ and of course $X_t^g \subset X_{t+\varepsilon}^f$.

If $F_t := \{\text{path connected components of } X_t^f\}$ and, analogously, $G_t := \{\text{path connected components of } X_t^g\}$, we induce the following commutative diagram:

$$\begin{array}{ccccccc}
 F_t & \xrightarrow{\alpha_t^{t+\varepsilon}} & F_{t+\varepsilon} & \xrightarrow{\alpha} & F_{t'} & \xrightarrow{\alpha} & F_{t'+\varepsilon} \\
 & \searrow & \nearrow & & \searrow & \nearrow & \\
 G_t & \xrightarrow{\beta_t^{t+\varepsilon}} & G_{t+\varepsilon} & \xrightarrow{\beta} & G_{t'} & \xrightarrow{\beta} & G_{t'+\varepsilon}
 \end{array}$$

We call $\widehat{\varphi} : F_t \rightarrow G_{t+\varepsilon}$ and $\widehat{\gamma} : G_t \rightarrow F_{t+\varepsilon}$. Note that the vertices of the merge trees associated to f and g are contained in some F_t or G_t respectively. The maps are all induced by inclusion and are defined in analogous ways on the basis of path connected components (p.c.c.). So we specify only $\widehat{\varphi}$:

$$(U \subset X_t^f \text{ p.c.c.}) \mapsto (V \subset X_{t+\varepsilon}^g \text{ p.c.c. containing } U)$$

To define $\widehat{\gamma}$ we simply exchange the role of f and g .

We indicate the path connected components of F_t with F_0^t, \dots, F_k^t and analogously for G_t . Since f and g are tame, we know that these are always finite. Clearly, we have that $\alpha_t^{t'}(F_i^t) = F_j^{t'}$ for some j . Usually we avoid the subscript and the superscript on α referring to its domain and codomain; if needed, we specify them.

If $\alpha_t^{t'}(F_i^t) = \alpha_t^{t'}(F_h^t) = F_j^{t'}$ then F_i^t and F_h^t have merged between t and t' . Similarly if $F_j^{t'} \notin \text{im}(\alpha_{t'}^{t'})$ then $F_j^{t'}$ is born between t' and t . Since f and g are tame, we know that merging and the birth of new components happens only in a finite set of critical points.

We recall that the leaves of the trees are associated to the birth of path-connected components, and the internal vertices of the trees to the points where components merge.

Given a path connected component $x \in F_t$, we can always find $t' = \min\{s \leq t \mid \# \alpha^{-1}(x) = 1\}$; we call $\Gamma_f(x)$ the preimage of x with $\alpha_{t'}^{t'}$. It is the closest point on the tree, going towards the leaves, in which x is involved in some merging. It is a way to associate to any component alive at time t , a vertex on the tree. In other words the function Γ_f maps any connected component of F_t (for any t), to a vertex of the tree T_f . An analogous map can be defined also for G_t and T_g ; call this functions Γ_g .

Having set notation, we now use it to establish some connections with merge trees as defined in Section 2.5.

Let T_f be the merge tree associated to f , with tree structure T and height function h_f ; similarly T_g is associated to g , with tree structure T' and height function h_g . Define the functions φ and γ , respectively by considering: $F_i^t \mapsto \Gamma_g(\widehat{\varphi}(F_i^t))$ or $G_i^t \mapsto \Gamma_f(\widehat{\gamma}(G_i^t))$. We will mainly use these functions restricted to the sets of vertices V_T and $V_{T'}$, to obtain

$$\varphi : V_T \rightarrow V_{T'}$$

$$v \mapsto \Gamma_g(\widehat{\varphi}(v))$$

$$\gamma : V_{T'} \rightarrow V_T$$

$$w \mapsto \Gamma_f(\widehat{\gamma}(w))$$

We now prove two lemmas which help in the proof of the theorem. We also introduce the following notation: given a vertex $v \in V_T$, then, the set ζ_v is the set $\zeta_v := \{v' \in V_T \mid v' \geq v\}$. In other words ζ_v collects all the points between v and r_T .

Lemma 1 Consider $v \in V_T$. If $|h_f(v) - h_g(\varphi(v))| > \varepsilon$, then there cannot be two or more distinct vertices v' and v'' such that $v = \min \zeta_{v'} \cap \zeta_{v''}$ with $h_f(v) - h_f(v') > \varepsilon$ and $h_f(v) - h_f(v'') > \varepsilon$. Moreover, for all vertices v''' in $\text{sub}_T(v)$ with $h_T(v) - h_T(v''') < \varepsilon$ we have $\varphi(v''') = \varphi(v)$.

Proof We prove this lemma by contradiction. Assume there are v' and v'' vertices which contradict the thesis.

Note that $\widehat{\varphi}(v')$ and $\widehat{\varphi}(v'')$ are less than or equal to $\varphi(v)$ in $V_{T'}$. But by hypothesis $h_g(\varphi(v)) < h_f(v) - \varepsilon$, which means that $h_f(\widehat{\gamma}(\varphi(v))) < h_f(v)$. Which is a contradiction because the components associated to v' and v'' cannot merge before $h_f(v)$.

The last part of the lemma follows because $h_g(\widehat{\gamma}(v''')) > h_g(\varphi(v))$. ■

Lemma 2 Consider F_i^t and $F_j^{t'}$ with $t < t'$ and $\varphi(F_i^t) = \varphi(F_j^{t'})$. Then $F_j^{t'}$ and $F_j^{t'}$ get merged before height $t' + 2\varepsilon$.

Proof If $\varphi(F_i^t) = \varphi(F_j^{t'})$ then $\widehat{\varphi}(F_i^t) \subset \widehat{\varphi}(F_j^{t'})$. This, in turn, implies that $\widehat{\gamma}(\widehat{\varphi}(F_i^t)) \subset \widehat{\gamma}(\widehat{\varphi}(F_j^{t'}))$ and so F_i^t and $F_j^{t'}$ get merged before height $t' + 2\varepsilon$. ■

Clearly the role of T and T' can be exchanged in the formulation of the lemmas.

Using these two lemmas we build a bottom-up procedure to turn T into T' via an edit path with at most one edit per vertex, each with cost less than 2ε .

Start from the leaves of T and order them according to increasing heights. If there are more leaves with the same height, order them at random. For each leaf v either (a) $|h_f(v) - h_g(\varphi(v))| > \varepsilon$ or (b) $|h_f(v) - h_g(\varphi(v))| \leq \varepsilon$ holds.

Consider the first leaf v . Since $|\min(f) - \min(g)| < \varepsilon$ then (b) must hold. Thus we take the couple $(v, \varphi(v))$. Consider now the second leaf v' . If (a) holds, then $\varphi(v') = \varphi(\widehat{\gamma}(\varphi(v')))$ and $h_f(v') > h_f(\widehat{\gamma}(\varphi(v')))$. Since v' is a leaf, then $\Gamma_f(\widehat{\gamma}(\varphi(v')))$ belongs to another branch, with respect to v' , since $h_f(v') > h_f(\widehat{\gamma}(\varphi(v')))$. Thus, by Theorem 2, v' can be deleted with cost at most 2ε . The same happens if $\varphi(v') = \varphi(v)$. Therefore, for each leaf v of T either we take the couple $(v, \varphi(v))$ - if (b) holds, and with vertices appearing in couples at most once - or we delete v with cost less than 2ε . Consider now the leaves of T' . If w is left uncoupled and (a) holds, then $\gamma(w) = \gamma(\widehat{\varphi}(\gamma(w)))$ with $w > \widehat{\varphi}(\gamma(w))$; reasoning as above, we deduce that w can be deleted with cost at most 2ε . If (b) holds, then $|h_g(w) - h_g(\varphi(\gamma(w)))| < 2\varepsilon$, since $|h_f(\gamma(w)) - h_g(\varphi(\gamma(w)))| < \varepsilon$. Thus we can delete w with cost less than 2ε in any case.

Therefore, we either couple or delete each leaf of T and T' .

These deletions may force some vertices to become leaves. Thus we can repeat recursively the same procedure until we obtain two merge trees whose leaves are all coupled. From such trees we remove all order two vertices. Since these trees are obtained from T and T' with deletions of cost less than 2ε and ghostings, if we prove the result for such trees the theorem is proven. So with an abuse of notation we call T and T' these new merge trees.

To conclude the proof we must first prove that the internal vertices of T and T' satisfy (b) and can be coupled respecting the tree structures.

Consider v an internal vertex of T and suppose $|h_f(v) - h_g(\varphi(v))| > \varepsilon$. Let v_1, \dots, v_n be its children. By hypothesis $n > 1$. We know that all the leaves in $\text{sub}_T(v_i)$ are coupled. In particular consider two leaves $v_a \in V_{\text{sub}_T(v_1)}$ and $v_b \in V_{\text{sub}_T(v_2)}$. We know that $\varphi(v_a) \neq$

$\varphi(v_b)$, and that those two components are merged in $\varphi(v)$. But then they are merged in $\widehat{\gamma}(\varphi(v))$ which has height less than $h_f(v)$; a contradiction. This of course holds also for T' .

Consider now the set $\varphi^{-1}(\varphi(v)) = \{v_1, \dots, v_n\}$. We know that for all i , $|h_f(v_i) - h_g(\varphi(v))| < \varepsilon$ and all the vertices get merged before $\max_i\{h_f(v_i)\} + \varepsilon$. Let $k = \operatorname{argmax}_i\{h_f(v_i)\}$. We can pair $(v_k, \varphi(v))$ and delete all other v_i , with cost less than 2ε . In this way we either couple or delete all vertices of T . Consider now $w \in V_{T'}$ which is left uncoupled. Since for w (b) holds, then $|h_g(w) - h_g(\varphi(\gamma(w)))| < 2\varepsilon$, because $|h_f(\gamma(w)) - h_g(\varphi(\gamma(w)))| < \varepsilon$. Thus we can delete all uncoupled vertices with deletions whose cost is less than 2ε .

In this way all vertices of T are either coupled, ghosted or deleted. Lastly, since $\widehat{\varphi}(v) \geq \widehat{\varphi}(v')$ then the coupling respects the tree structures of T and T' . Therefore, once we delete all vertices which are not coupled, and remove all order 2 vertices, we obtain from T and T' two trees with isomorphic tree structures - the isomorphism being φ . Again to avoid the introduction of new notation, we call these trees T and T' . At this point we can interpret the couples $(v, \varphi(v))$ as defining shrinkings. Let $e = (v, v')$, $w_T(e) = h_f(v') - h_f(v)$, $e' = (\varphi(v), \varphi(v'))$ and $w_{T'}(e') = h_g(\varphi(v), \varphi(v'))$. Since $|h_f(v) - h_g(\varphi(v))| < \varepsilon$ and $|h_f(v') - h_g(\varphi(v'))| < \varepsilon$, then $\operatorname{cost}((v, \varphi(v))) = |w_T(e) - w_{T'}(e')| < 2\varepsilon$. ■

A.1 Combining Metrics

To aggregate curvature and radius, we make use of the following Proposition.

Proposition 3 *Given (X, d_0) and (X, d_1) metric spaces, then $d_{a,b,p} := (a \cdot d_0^p + b \cdot d_1^p)^{1/p}$, with $a, b \in \mathbb{R}_{>0}$ and $p \geq 1$, is a metric on X .*

Proof

$$d_{a,b,p}(x, y) = \|(a^{1/p} \cdot d_0(x, y), b^{1/p} \cdot d_1(x, y))\|_p.$$

Since, given $k > 0$, $k \cdot d_i$ is a metric if and only if d_i is a metric, we can rescale d_0 and d_1 and take $a = b = 1$. We refer to $d_{1,1,p}$ as d_p .

So:

- $d_p(x, y) = 0$ iff $d_0(x, y) = 0 = d_1(x, y)$ and this happens if and only if $x = y$.
- symmetry is obvious
- we use $\|h+q\|_p \leq \|h\|_p + \|q\|_p$ with $h = (d_0(x, z), d_1(x, z))$ and $q = (d_0(z, y), d_1(z, y))$.

Since $d_i(x, y) \leq d_i(x, z) + d_i(z, y)$ we get:

$$\|(d_0(x, y), d_1(x, y))\|_p \leq \|(d_0(x, z) + d_0(z, y), d_1(x, z) + d_1(z, y))\|_p = \|(d_0(x, z), d_1(x, z)) + (d_0(z, y), d_1(z, y))\|_p \leq \|(d_0(x, z), d_1(x, z))\|_p + \|(d_0(z, y), d_1(z, y))\|_p.$$

Therefore:

$$d_p(x, y) \leq d_p(x, z) + d_p(z, y). ■$$

References

H. Adams, Tegan Emerson, M. Kirby, R. Neville, C. Peterson, P. Shipman, Sofya Chepushtanova, E. Hanson, F. Motta, and Lori Ziegelmeier. Persistence images: A stable vector representation of persistent homology. *J. Mach. Learn. Res.*, 18:8:1–8:35, 2017.

Kenes Beketayev, Damir Yeliussizov, Dmitriy Morozov, Gunther H. Weber, and Bernd Hamann. Measuring the distance between merge trees. In *Topological Methods in Data Analysis and Visualization*, 2014.

Subhrajit Bhattacharya, Robert Ghrist, and Vijay Kumar. Persistent homology for path planning in uncertain environments. *IEEE Transactions on Robotics*, 31:1–13, 06 2015. doi: 10.1109/TRO.2015.2412051.

Silvia Biasotti, Daniela Giorgi, Michela Spagnuolo, and Bianca Falcidieno. Reeb graphs for shape analysis and applications. *Theoretical Computer Science*, 392:5–22, 02 2008. doi: 10.1016/j.tcs.2007.10.018.

Philip Bille. A survey on tree edit distance and related problems. *Theoretical computer science*, 337(1-3):217–239, 2005.

Peter Bubenik. Statistical topological data analysis using persistence landscapes. *Journal of Machine Learning Research*, 16(3):77–102, 2015.

F. Chazal, Brittany Terese Fasy, F. Lecci, A. Rinaldo, and L. Wasserman. Stochastic convergence of persistence landscapes and silhouettes. *J. Comput. Geom.*, 6:140–161, 2015.

Moo K. Chung, Peter Bubenik, and Peter T. Kim. Persistence diagrams of cortical surface data. In Jerry L. Prince, Dzung L. Pham, and Kyle J. Myers, editors, *Information Processing in Medical Imaging*, pages 386–397, Berlin, Heidelberg, 2009. Springer Berlin Heidelberg. ISBN 978-3-642-02498-6.

D. Cohen-Steiner, H. Edelsbrunner, and J. Harer. Stability of persistence diagrams. *Discrete & Computational Geometry*, 37:103–120, 2007.

David Cohen-Steiner, Herbert Edelsbrunner, John Harer, and Yuriy Mileyko. Lipschitz functions have l^p -stable persistence. *Foundations of Computational Mathematics*, 10: 127–139, 02 2010. doi: 10.1007/s10208-010-9060-6.

Carl De Boor and James W Daniel. Splines with Nonnegative B-spline Coefficients. *Mathematics of computation*, 28(126):565–568, 1974.

I. L. Dryden and K. V. Mardia. *Statistical Shape Analysis*. Wiley, Chichester, 1998.

H. Edelsbrunner, D. Letscher, and A. Zomorodian. Topological persistence and simplification. *Discrete & Computational Geometry*, 28:511–533, 2002.

Herbert Edelsbrunner and John Harer. Persistent homology-a survey. *Contemporary mathematics*, 453:257–282, 2008.

Frédéric Ferraty and Philippe Vieu. *Nonparametric functional data analysis: theory and practice*. Springer Science & Business Media, 2006.

Ellen Gasparovic, E. Munch, S. Oudot, Katharine Turner, B. Wang, and Yusu Wang. Intrinsic interleaving distance for merge trees. *ArXiv*, abs/1908.00063, 2019.

Allen Hatcher. *Algebraic topology*. Cambridge Univ. Press, Cambridge, 2000.

Eunpyeong Hong, Yasuaki Kobayashi, and Akihiro Yamamoto. Improved methods for computing distances between unordered trees using integer programming. In *International Conference on Combinatorial Optimization and Applications*, pages 45–60. Springer, 2017.

Miroslav Kramár, Arnaud Goullet, Lou Kondic, and K Mischaikow. Persistence of force networks in compressed granular media. *Physical review. E, Statistical, nonlinear, and soft matter physics*, 87:042207, 04 2013. doi: 10.1103/PhysRevE.87.042207.

Barry Lavine and Jerome Workman. Chemometrics. *Analytical chemistry*, 80(12):4519–4531, 2008.

J. S. Marron, J. Ramsay, L. Sangalli, and A. Srivastava. Statistics of time warpings and phase variations. *Electronic Journal of Statistics*, 8:1697–1702, 2014.

J. S. Marron, J. Ramsay, L. Sangalli, and A. Srivastava. Functional data analysis of amplitude and phase variation. *Statistical Science*, 30(4):468–484, 2015.

Peter Michor, David Mumford, Jayant Shah, and Laurent Younes. A metric on shape space with explicit geodesics. *Atti Accad. Naz. Lincei Cl. Sci. Fis. Mat. Natur. Rend. Lincei (9) Mat. Appl.*, 19, 07 2007. doi: 10.4171/RLM/506.

D. Morozov and G. Weber. Distributed merge trees. In *PPoPP '13*, 2013.

Dmitriy Morozov, Kenes Beketayev, and Gunther Weber. Interleaving distance between merge trees. *Discrete and Computational Geometry*, 49:22–45, 01 2013.

Florian Pokorny, Majd Hawasly, and Subramanian Ramamoorthy. Topological trajectory classification with filtrations of simplicial complexes and persistent homology. *The International Journal of Robotics Research*, 35, 08 2015. doi: 10.1177/0278364915586713.

James O. Ramsay and Bernard W. Silverman. *Functional Data Analysis*. Springer, New York, NY, USA, 2005.

B. Ripley and U. Grenander. General pattern theory: A mathematical theory of regular structures. *Journal of the Royal Statistical Society. Series A (Statistics in Society)*, 158: 635, 01 1995. doi: 10.2307/2983457.

L. Sangalli, P. Secchi, and S. Vantini. Analysis of aneurisk65 data: \$k\$-mean alignment. *Electronic Journal of Statistics*, 8:1891–1904, 2014.

Laura Sangalli, Piercesare Secchi, Simone Vantini, and Alessandro Veneziani. Efficient estimation of three-dimensional curves and their derivatives by free-knot regression splines, applied to the analysis of inner carotid artery centrelines. *Journal of the Royal Statistical Society Series C*, 58:285–306, 07 2009a. doi: 10.1111/j.1467-9876.2008.00653.x.

Laura Sangalli, Piercesare Secchi, Simone Vantini, and Valeria Vitelli. K-mean alignment for curve clustering. *Computational Statistics & Data Analysis*, 54:1219–1233, 05 2010. doi: 10.1016/j.csda.2009.12.008.

Laura M. Sangalli, Piercesare Secchi, Simone Vantini, and Alessandro Veneziani. A case study in exploratory functional data analysis: Geometrical features of the internal carotid artery. *Journal of the American Statistical Association*, 104(485):37–48, 2009b.

Y. Shinagawa, T. L. Kunii, and Y. L. Kergosien. Surface coding based on morse theory. *IEEE Computer Graphics and Applications*, 11(5):66–78, 1991.

R. Sridharamurthy, T. B. Masood, A. Kamakshidasan, and V. Natarajan. Edit distance between merge trees. *IEEE Transactions on Visualization and Computer Graphics*, 26(3):1518–1531, 2020.

A. Srivastava, I. Jermyn, and Shantanu H. Joshi. Riemannian analysis of probability density functions with applications in vision. *2007 IEEE Conference on Computer Vision and Pattern Recognition*, pages 1–8, 2007.

A. Srivastava, W. Wu, S. Kurtek, E. Klassen, and J. S. Marron. Registration of functional data using fisher-rao metric. *arXiv: Statistics Theory*, 2011.

Anuj Srivastava, Eric Klassen, Shantanu Joshi, and Ian Jermyn. Shape analysis of elastic curves in euclidean spaces. *IEEE transactions on pattern analysis and machine intelligence*, 09 2010. doi: 10.1109/TPAMI.2010.184.

Elena Farahbakhsh Touli. Frechet-like distances between two merge trees. *ArXiv*, abs/2004.10747, 2020.

Elena Farahbakhsh Touli and Yusu Wang. Fpt-algorithms for computing gromov-hausdorff and interleaving distances between trees. In *ESA*, 2018.

Simone Vantini. On the definition of phase and amplitude variability in functional data analysis. *Test*, 21:1–21, 01 2009. doi: 10.1007/s11749-011-0268-9.

Yuan Wang, Hernando Ombao, and Moo Chung. Topological data analysis of single-trial electroencephalographic signals. *The Annals of Applied Statistics*, 12:1506–1534, 09 2018. doi: 10.1214/17-AOAS1119.

Kelin Xia, Zhiming Li, and Lin Mu. Multiscale persistent functions for biomolecular structure characterization. *Bulletin of Mathematical Biology*, 80, 12 2016. doi: 10.1007/s11538-017-0362-6.

Qunqun Yu, Xiaosun Lu, and J. S. Marron. Principal nested spheres for time-warped functional data analysis. *Journal of Computational and Graphical Statistics*, 26:144 – 151, 2013.